

# **Developments in Soluble Lead Flow Batteries and Remaining Challenges: An Illustrated Review**

M. Krishna\*, E.J. Fraser, R.G.A. Wills, F.C. Walsh

Electrochemical Engineering Laboratory, Energy Technology Research Group, Faculty of Engineering and the Environment, University of Southampton, SO17 1BJ, UK

\*Corresponding Author

[m.k.krishna@soton.ac.uk](mailto:m.k.krishna@soton.ac.uk)

## **Abstract**

The soluble-lead flow battery (SLFB) utilises methanesulfonic acid, an electrolyte in which Pb(II) ions are highly soluble. During charge, solid lead and lead dioxide layers are electrodeposited at the negative and positive electrodes respectively. During discharge, the deposits are electrochemically dissolved back into the recirculating electrolyte. The cell is normally undivided, which greatly reduces design complexity and cost, whilst also reducing the flow pumping requirements. Typical SLFB electrolytes offer up to 40 W h kg<sup>-1</sup> of storage, with performance on the 100 cm<sup>2</sup> electrode scale reaching 90% charge and 80% voltage efficiencies across 100 cycles; however the SLFB has also been tested on the 1000 cm<sup>2</sup> electrode, four-cell stack scale. This review considers the SLFB, highlighting important developments and discussing remaining problems. In particular, methods to achieve effective stripping of lead dioxide at the positive electrode and to prevent lead dendrites at the negative electrode in order to prevent contact between the deposits, and thus shorting, are explored. A detailed understanding of the effect of Pb(II) and methanesulfonic acid concentration on the physical electrolyte properties is presented, and possible improvements to the electrodes and electrolyte composition in terms of additives are discussed in order to improve cell efficiency and longevity. Also, the importance of cell design in preventing the failure mechanisms and therefore achieving a high performance is

highlighted. Studies on mathematical modelling and cycling simulation are also reviewed. Continuing research needs are listed and a forward look to future developments is taken.

**Keywords:** electrolyte additives, soluble lead, lead dioxide, methanesulfonic acid, redox flow battery

## Contents

<b>Abstract</b>	<b>1</b>
<b>1 Introduction</b>	<b>5</b>
1.1 The Scope of this Review	5
1.2 The soluble lead redox flow battery	6
1.3 Constraints on the system	8
1.4 Brief history of lead-based batteries	9
<b>2 Thermodynamics and storage capacity</b>	<b>14</b>
<b>3 Deposit and electrolyte properties</b>	<b>16</b>
3.1 Lead	16
3.2 Lead dioxide	16
3.3 Methanesulfonic acid	17
3.4 Electrolyte density and viscosity	19
3.5 Electrolyte conductivity	19
<b>4 Electrode kinetics</b>	<b>20</b>
4.1 Negative redox couple	20
4.2 Positive redox couple	21
<b>5 Operating conditions</b>	<b>23</b>
5.1 Negative electrode	23
5.2 Positive electrode	27

5.3	Further discussion on the structure of lead dioxide	30
5.4	Potential–time plots	32
5.5	Discharge at the positive electrode	33
5.6	Further observations at the positive electrode	35
5.7	Flow rate	36
<b>6</b>	<b>Additives</b>	<b>37</b>
6.1	Negative electrode	37
6.2	Positive electrode	38
<b>7</b>	<b>Electrode materials</b>	<b>40</b>
<b>8</b>	<b>Electrolyte composition</b>	<b>43</b>
8.1	Conventional electrolyte	43
8.2	Recycled electrolyte	44
<b>9</b>	<b>Performance</b>	<b>44</b>
9.1	Flow cells	44
9.2	Flow battery	46
<b>10</b>	<b>Flow cell engineering</b>	<b>47</b>
10.1	Cell design	47
10.2	Cell maintenance	50
<b>11</b>	<b>Modelling and simulation</b>	<b>52</b>
<b>12</b>	<b>Summary and future work</b>	<b>54</b>
	<b>References</b>	<b>58</b>

# 1 Introduction

## 1.1 The Scope of this Review

With the growing global energy demand, energy storage will become a key component in maintaining a dependable energy supply whilst integrating renewables into electricity networks. Energy storage devices, by electrochemical or mechanical means, have been reviewed extensively, including those by Chen *et al.* [1] and Akhil *et al.* at the Sandia National Laboratories [2].

Redox flow batteries have been growing in popularity since modern research began in the 1970s [3]. A multitude of battery chemistries exists today, with the vanadium redox flow battery (VRFB) being the most advanced. These have also been reviewed in detail, including their operational principles and remaining technical challenges [4-7]. Furthermore, a review focusing on the engineering aspects of flow batteries has been published by Arenas *et al.* [8] and Chalamala *et al.* [9]. The largest operational flow battery installation is the SEI 15 MW/60 MWh VRFB used for renewables capacity firming in Hokkaido, Japan [10]. Flow batteries are readily scalable, and the VRFB has been shown possess efficiencies >90%, lifetimes of 20 years, low initial costs (the cost per kW decreases with greater storage capacity), robust construction, low maintenance and flexible operation. Safety is another key feature of flow batteries, which typically operate at ambient temperature.

A flow battery consists of several cells connected electrically in series, typically as a bipolar stack. In the general design, a flow cell is divided into two half-cells via a separator. The positive electrolyte and negative electrolyte are housed separately in external tanks and two flow networks circulate the electrolytes through the respective half-cells. The cell electrodes are connected externally to a power source/load. When power is supplied, the cell charges: electrochemical reactions occurring at the electrodes' surface cause a change in the oxidation states of the reactant species in the electrolyte.

Energy is stored as these new, 'charged' species. On discharge, the reactions are reversed and the stored energy is released.

Research continues today to improve performance whilst reducing costs, and one such chemistry that has shown much promise is the soluble lead system. This review will focus solely on the soluble lead redox flow battery (SLFB). The concept of a SLFB and its differences with conventional static lead-acid batteries are discussed. A thermodynamic perspective of the chemical processes will be presented along with theoretical cell voltages. The review will critically assess the problems that hinder the SLFB's progression to a commercialisation stage and the work that has been done to mitigate these problems. Further aspects requiring development and recent improvements will also be discussed including summary data from voltammetry and several galvanostatic charge/discharge experiments. The task of optimising electrolyte concentrations and charge regimes will be discussed following a comprehensive analysis of each electrode reaction. Where relevant, experience from the coatings industry and other forms of flow batteries are also discussed in relation to the SLFB.

## **1.2 The soluble lead redox flow battery**

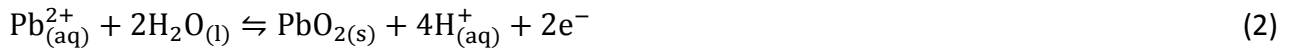
The SLFB makes use of the variable oxidation states of lead, namely Pb, Pb(II) and Pb(IV). Electrolytes are formulated either from lead oxide, lead carbonate or aqueous lead methanesulfonate,  $\text{Pb}(\text{CH}_3\text{SO}_3\text{H})_2$  and methanesulfonic acid (MSA),  $\text{CH}_3\text{SO}_3\text{H}$ . In the simplest SLFB design,  $\text{Pb}^{2+}$  ions are dissolved in an aqueous MSA solution and this electrolyte is then pumped through an undivided electrochemical cell. During charge, at the positive electrode,  $\text{Pb}^{2+}$  is oxidised and a phase change occurs, leading to the deposition of lead dioxide on the electrode. At the negative electrode  $\text{Pb}^{2+}$  is reduced, with an associated phase change resulting in metallic lead deposition onto the electrode. During discharge, the electrodeposits dissolve back into the electrolyte [11]. This is described by the following equations:

### Negative electrode



$$E_{-\text{ve}}^{\circ} = -0.130 \text{ V vs. SHE}$$

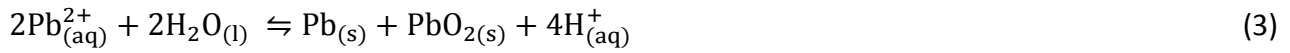
### Positive electrode



$$\alpha - \text{PbO}_2 \quad E_{+\text{ve}}^{\circ} = +1.468 \text{ V vs. SHE}$$

$$\beta - \text{PbO}_2 \quad E_{+\text{ve}}^{\circ} = +1.460 \text{ V vs. SHE}$$

### Cell Reaction



$$E_{\text{cell}}^{\circ} = +1.598 \text{ V}$$

The standard potentials for  $\text{Pb}^{2+}/\alpha\text{-PbO}_2$  and  $\text{Pb}^{2+}/\beta\text{-PbO}_2$  are 1.468 V [12] and 1.46 V [13], respectively. At almost 1.6 V, the standard equilibrium cell potential is higher than that of the VRFB at 1.26 V and comparable to that of the zinc-bromine redox flow battery (ZBFB) at 1.85 V [4]. From these equations, it can be seen that the electrolyte composition is constantly changing during battery operation.  $\text{Pb}^{2+}$  concentration decreases during charge whilst the acidity increases, as two moles of  $\text{H}^{+}$  are released per mole of  $\text{Pb}^{2+}$  deposited. The volume of electrolyte and concentration of  $\text{Pb}^{2+}$  along with the thickness of lead and lead dioxide that is achievable on the electrodes dictates the storage capacity. The electrode chemistries are different to the conventional lead-acid battery as there is no insoluble  $\text{Pb}^{2+}$  in the form of lead sulfate. A simplified SLFB cell design is shown in Figure 1.

## FIGURE 1 NEAR HERE

Unlike other flow battery chemistries, the SLFB uses an electrolyte common to both electrode reactions and therefore a separator is not required. There is only one electrolyte tank and one set of pipework, which greatly simplifies the design and cost of the system. There is no problem of electrolyte crossover, and fewer cell components reduces the likelihood of leakage. Electrode degradation seen in the VRFB [4] could also be avoided, as electrodes in the SLFB soon acquire passivating lead and lead dioxide deposits.

### 1.3 Constraints on the system

The electrolyte and electrodes in the ideal SLFB will be able to return to their initial states after every full discharge stage over a variety of temperatures and current densities, i.e. the lead and lead dioxide deposits should be uniform, compact, thick and adhere well to the substrate whilst also being able to electrochemically re-dissolve fully back into the electrolyte as  $\text{Pb}^{2+}$  ions. This should continue for many cycles before maintenance is required and no secondary reactions, such as  $\text{H}_2/\text{O}_2$  evolution would occur. The battery should also be able to fully discharge at high rates whilst still maintaining its voltage and without any long-lasting damage. For all this to occur, both electrode reactions must have equal and high charge efficiencies (>95%). Losses such as leakage currents and internal resistances should be low so as to minimise the electrode overpotentials, and this all should be achieved with minimal ancillary losses, such as temperature control, power management and electrolyte pumping (i.e. low solution viscosity and minimal pressure drop over the flow path).

There are challenges for both the half-cells in the SLFB. Whilst lead deposition and stripping is highly efficient at the negative electrode [14], it does require a surfactant in the electrolyte to avoid the



tendency to deposit rough, cauliflower-like crystal structures which can be a precursor to dendritic growth. These nodular growths are prone to being knocked off the electrode by the flowing electrolyte, leading to a loss in energy capacity, and can even grow across the side of the internal cell wall towards the positive electrode, where electrical shorting can occur if contact is made. This will also lead to a loss in energy capacity [15]. It is important, therefore, to be able to deposit uniform, compact deposits at both electrodes.

At the positive electrode, the  $\text{Pb}^{2+}/\text{PbO}_2$  redox couple suffers from slow reaction kinetics and much higher overpotentials than the negative electrode [14]. The poor reversibility of the  $\text{Pb}^{2+}/\text{PbO}_2$  couple is the main limitation of the system and over prolonged battery cycling, leads to the build-up of deposits at both electrodes, depleting the solution of the electroactive species,  $\text{Pb}^{2+}$ . These deposits cannot be dissolved via conventional cell discharge and will need to be forcibly removed by either applying power or dismantling the cell and physically removing the deposits.  $\text{PbO}_2$  deposits can also creep across non-conducting surfaces, such as the cell's internal walls or inlet/outlet flow distributor, causing shorting [16, 17]. In addition, cracks can form on the  $\text{PbO}_2$  surface, causing flaking of the deposit. These insoluble, fallen deposits accumulate as sludge at the bottom of the cell and can block the flow-field.

#### **1.4 Brief history of lead-based batteries**

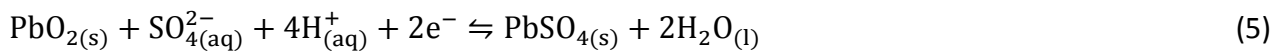
The supporting electrolyte and operational principle of the standard lead-acid battery (LAB) are fundamentally different to the SLFB. The simplest form of the LAB is known as a flooded cell, which consists of solid lead (negative) and lead dioxide (positive) electrodes immersed in a static sulfuric acid solution. The electrodes are kept apart by the use of a separator, and lead and its compounds remain insoluble throughout operation; both electrodes are converted to lead sulfate on discharge and this is reversed on charge according to the following reactions [18]:

### Negative electrode



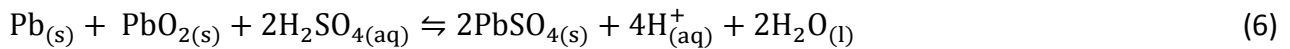
$$E_{-ve}^{\circ} = -0.358 \text{ V vs. SHE}$$

### Positive electrode



$$E_{+ve}^{\circ} = +1.683 \text{ V vs. SHE}$$

### Cell reaction



$$E_{\text{cell}}^{\circ} = +2.041 \text{ V}$$

The high reversibility of the forward reactions under different loads, the low cost of lead and sulfur, the design simplicity and a high cycle life, amongst other advantages, have contributed to the success of the LAB [19]. LABs are used for starting, lighting and ignition (SLI) applications, for example in automobiles where high surge currents are required for short durations. The batteries can also be scaled up for UPS services as well as load levelling and increasing the robustness of renewables. The largest LAB installation is the 36 MW/24 MW h array at the 153 MW Notrees wind power project in Texas, USA [10].

Since its inception in 1859 by Gaston Planté, the LAB has undergone over 150 years of development. The world's first fully electric car in 1881 and submarine in 1886 were powered by LABs. In 1899,

Jenatzy's LAB-powered automobile was able to surpass a speed of  $100 \text{ km h}^{-1}$ . As the World's portable power demands grew, breakthroughs in manufacturing in 1898 by Barton and 1926 by Shimadzu paved the way for industrial scale production of LABs [18].

In the early second half of the 20th century, the valve-regulated lead-acid battery (VRLAB) was designed. There are two common forms of VRLAB: the absorbed glass mat (AGM), where the electrolyte is held within the pores of the glass mat separator, and the undivided gel battery, where silica is used to create a highly viscous gel-like electrolyte [20]. These designs brought many improvements to the flooded system: the recharge time and self-discharge rate was decreased, and the cycle life and specific power was increased. Safety was also substantially improved: any evolution of hydrogen and oxygen was forced to recombine back into water, and in case this process did not occur rapidly enough, valves safely released any internal pressure build-up. Deeper cycles could also be achieved and maintenance became obsolete as the battery became self-regulating.

VRLABs offer a low specific energy and specific power, about  $30\text{-}40 \text{ W h kg}^{-1}$  and  $180 \text{ W kg}^{-1}$ , respectively which is much lower than the lithium-ion batteries currently used to power electric cars, which can offer a specific energy of  $160 \text{ W h kg}^{-1}$  and a specific power of  $1800 \text{ W kg}^{-1}$  [18]. However, lead batteries continue to be a popular area of research and advanced lead-acid batteries have shown significant improvements. Amongst these is the Ultrabattery, which was developed by CSIRO in 2006. Early studies showed that, by combining a supercapacitor alongside the lead electrode in a single cell, the charge and discharge power can be improved by 50% and the cycle life tripled [21]. These promising results have invoked interest in using these batteries for hybrid-electric vehicles. Figure 2 summarises the key milestones in LAB development and the main stages of SLFB research. A detailed comparison between the LAB and SLFB, including performance, can be found in the work by Zhang *et al.* [22].

## FIGURE 2 NEAR HERE

The earliest record of battery research involving a soluble lead species dates back to the late 1940s [17]. These were primary batteries that used mostly solid lead negative electrodes and positive electrodes consisting of a lead dioxide coating [23, 24]. The supporting electrolyte used perchloric, fluoroboric or fluorosilicic acid, having taken inspiration from the lead plating industry at the time [25]. They were designed for small-scale, short term emergency applications, where the dry cell would be filled with acid just before operation. Of these early primary battery patents, the lead dioxide electrode was prepared by deposition onto a nickel substrate using a circulated lead nitrate solution [23].

Later in the 1970s and early 80s, several patents for secondary box, button and flow cells were filed [26-28]. Hexafluorosilicic and amidosulfonic acids were introduced, again taken from the plating industry. A circulated electrolyte through a stack incorporating bipolar electrodes was used for the first time by Wurmb *et al.* [27] with the motivation of obtaining greater efficiency, higher current density and better performance than lead-acid batteries at the time. The SLFB's current problems regarding the reversibility of lead dioxide deposition were also first identified and various operating conditions, additives and electrode structures were recommended to minimise these issues. The phasing out of lead silicofluoride in favour of lead methanesulfonate began with Henk *et al.* [28], who also focused on producing bespoke graphite electrodes.

Further developments were later made during the 2000s by several groups. Wills *et al.* reported the use of a small flow cell with an active electrode area of 2 cm<sup>2</sup> [11, 15, 29, 30] and 8 cm<sup>2</sup> in studies supported by Regenesys Technologies Ltd [31, 32]. Methanesulfonic acid became the preferred

supporting electrolyte, following the trend in the plating industry. Larger cells with active electrode areas of  $64\text{ cm}^2$  and  $100\text{ cm}^2$  were introduced soon after and scaled up in collaboration with C-Tech Innovation Ltd [16, 17, 33, 34]. The initial papers carried out proof-of-concept studies regarding electrode kinetics [11], electrode materials and flowing electrolytes [29, 30], electrolyte composition and additives [15, 31-33], whilst the later papers focused on system scale up [16, 17]. There has also been work published on modelling of the system [35]. In 2006, a Nafion membrane was used to divide the positive and negative half-cells in the soluble lead flow cell (amongst other chemistries) and patented by Clarke *et al.* [36]. However, the reasons for this are unclear, the system design is vague, no electrode-specific additives are mentioned and few performance metrics are given.

2000 1-hr cycles at 95% charge and 79% voltage efficiency were achieved by Verde *et al.* [37] in a beaker-cell study in 2013, indicating the potential of the soluble lead system. The  $\text{Pb}^{2+}/\text{PbO}_2$  couple has attracted further attention: Velichenko *et al.* [38] have studied in depth the multi-stage process of lead dioxide deposition from MSA solutions (Section 4.2), whilst Pletcher *et al.* [33] have studied the effect of the electrolyte conditions on the morphology of lead dioxide (Section 5.2). The SLFB continues to be a promising area of flow battery research and efforts now are focused on the reversibility of the positive electrode reaction and the scaling up of the system.

## 2 Thermodynamics and storage capacity

The change in the Gibbs Free Energy of the cell,  $\Delta G_{cell}^o$ , on discharge under standard conditions is - 308 kJ mol<sup>-1</sup>. The Nernst equation, using the concentration rather than the activity of the active species, can be used to approximate the equilibrium potentials for the positive and negative electrodes of the SLFB system under non-standard conditions:

$$E_{-ve}^e = E_{-ve}^o + \frac{RT}{zF} \ln [\text{Pb}^{2+}] \quad \text{Negative electrode} \quad (7)$$

$$E_{+ve}^e = E_{+ve}^o + \frac{RT}{zF} \ln \frac{[\text{H}^+]^4}{[\text{Pb}^{2+}]} \quad \text{Positive electrode} \quad (8)$$

$$E_{cell}^e = E_{cell}^o + \frac{RT}{zF} \ln \frac{[\text{H}^+]^4}{[\text{Pb}^{2+}]^2} \quad \text{Overall cell} \quad (9)$$

Where  $E_{+ve}^e$  is the standard electrode potential,  $R$  the universal gas constant (8.314 J mol<sup>-1</sup> K<sup>-1</sup>),  $T$  is the temperature,  $z$  is the electron equivalent per mole of reactant (i.e. the number of valent electrons in the stoichiometric equation,  $z = 2$  in the SLFB reactions) and  $F$  is Faraday's constant (96485 C mol<sup>-1</sup>). The units of  $zF$  together are C mol<sup>-1</sup>.  $[\text{H}^+]$  and  $[\text{Pb}^{2+}]$  are the concentrations of protons and lead ions in mol dm<sup>-3</sup>.  $E_{cell}^e$  is the open-circuit cell potential. There is zero net current flow at this potential, and it is equivalent to the minimum achievable cell potential on charge and the maximum achievable cell potential on discharge. At higher SoC, due to the higher  $[\text{H}^+]$  and lower  $[\text{Pb}^{2+}]$  in solution,  $E_{cell}^e$  will be higher than at a lower SoC. Table 1 compares the standard potentials and  $\Delta G_{cell}^o$

with those of other batteries, where it can be seen that  $\Delta G_{cell}^o$  in the SLFB is more than twice as high in the VRFB and comparable with the ZBFB.

### TABLE 1 NEAR HERE

The specific energy of a soluble lead electrolyte, in W h kg<sup>-1</sup> (per kg electrolyte),  $E_s$  can be calculated from

$$E_s = \frac{1}{2} \cdot \frac{zFE_{dc}[\text{Pb}^{2+}]}{3600\rho} \quad (10)$$

where  $E_{dc}$  is the nominal cell discharge potential in V,  $\rho$  is the density of the electrolyte in kg dm<sup>-3</sup> and 3600 represents s h<sup>-1</sup>. The 1/2 is included here since one unit of charge deposits an equivalent amount of lead and lead dioxide. The specific energy of the VRFB is limited by the low solubility of the vanadium species, typically offering 25 – 30 W h kg<sup>-1</sup> (electrolyte) [6] of storage energy. The zinc-bromine flow battery (ZBFB), the only other commercially available flow battery, offers higher specific energies of around 65 – 75 W h kg<sup>-1</sup> (per kg electrolyte). SLFB electrolytes favoured by Wills *et al.* [17] possess a higher specific energy than the VRFB (though lower than the ZBFB), at 40 W h kg<sup>-1</sup> (per kg electrolyte).

It would also be useful to relate the thickness of the deposits to the charge passed through the system or the amount of molar conversion. Assuming perfectly uniform deposition onto 2D electrodes, the general formula for calculating the thickness of any electrodeposit,  $d$  in cm, as a function of molar conversion is given by

$$d = \frac{Mnq\phi}{A\rho zF} \quad (11)$$

where  $M$  is the molar mass in  $\text{g mol}^{-1}$ ,  $\rho$  is the deposit density in  $\text{g cm}^{-3}$ ,  $A$  is the electrode area in  $\text{cm}^2$ ,  $n$  is amount of moles of  $\text{Pb}^{2+}$  converted to solid Pb or  $\text{PbO}_2$  at an electrode surface,  $q$  is the total charge passed through the system in C and  $\phi$  is the current (or Faradaic) efficiency of the system, which is the proportion of current used for the main reaction to the overall current supplied. Assuming  $\phi = 1$ , the lead dioxide deposit will theoretically always be 1.4 times thicker than the lead deposit.

### 3 Deposit and electrolyte properties

#### 3.1 Lead

Lead has an atomic number of 82 and a molar mass of  $207.21 \text{ g mol}^{-1}$ . Solid lead is soft, malleable and has a high corrosion resistance. It is a bluish-silver coloured heavy metal with a high density of  $11.337 \text{ g cm}^{-3}$  and a low melting point of  $327.5 \text{ C}$  [39]. Lead has a high hydrogen evolution overpotential, which is an important benefit as a battery material. This is due to the weakness of the Pb-H bond: placed at the lower left of the volcano plot for hydrogen evolution, this bond strength is  $113 \text{ kJ mol}^{-1}$  compared to  $197 \text{ kJ mol}^{-1}$  for Ni and  $225 \text{ kJ mol}^{-1}$  for Pt near the peak of the volcano plot [40].

#### 3.2 Lead dioxide

Lead dioxide (lead(IV) oxide) has a molar mass of  $239.21 \text{ g mol}^{-1}$ . It is black in colour and has a crystalline structure with two allotropes, the  $\alpha$  and  $\beta$  phase [18]. The density of plattnerite, the natural mineral form of  $\beta\text{-PbO}_2$ , is  $9.375 \text{ g cm}^{-3}$  [39]. The densities of  $\alpha\text{-PbO}_2$  and  $\beta\text{-PbO}_2$  found in the



electrode of the LAB are  $9.72 \text{ g cm}^{-3}$  and  $9.57 \text{ g cm}^{-3}$ , respectively [18].

Despite lead dioxide coatings having been studied for well over a century, the deposition mechanism is still debated; the most popular theory being presented in Section 4.2. Apart from the conversion to  $\text{PbSO}_4$  in the LAB, there is relatively little research concerning the reduction of lead dioxide to  $\text{Pb}^{2+}$ . Lead dioxide has been studied so extensively for coatings because of its many useful properties, which includes high electrical conductivity (the  $\beta$  phase is comparable to that of titanium), high oxygen evolution overpotential and good chemical stability in corrosive media; all important qualities for battery operation [41].

The  $\alpha$  phase has an orthorhombic shape with compact packing of the particles, whilst the  $\beta$  phase is tetragonal in nature, consisting of rough and larger, overlapping crystals [42]. The greater porosity of the  $\beta$  phase provides a higher surface area, making it well-suited for applications such as the oxidation of organic compounds in waste water treatment [43]. The effect of differing proportions of  $\alpha$  and  $\beta$  in the LAB is also well understood, though the conditions affecting their respective formations from MSA media remains unclear (Section 5.2). It has been suggested that the more-compact and smoother surface morphology of deposited  $\alpha\text{-PbO}_2$  makes it the preferred form in the SLFB [33]. However, recent experiments may have cast doubt on this theory (Sections 5.3 and 5.5).

From the potential-pH diagram of the lead-water system [44], it can be seen that  $\text{PbO}$  and other lead oxide compounds are formed in moderately alkaline conditions. This has been reported in practice, where deep within the lead dioxide deposit in the SLFB [30], and also the positive electrode in the LAB, proton starvation can lead to the formation of  $\text{PbO}$  [16].

### **3.3 Methanesulfonic acid**

MSA is a strong acid with a  $pK_a$  value of -1.8 [45]. It is completely ionised at 0.1 M in aqueous solution [46], where it dissociates into  $H^+$  and the methanesulfonate anion  $CH_3SO_3^-$ . It has a molar mass of  $96.11 \text{ g mol}^{-1}$  and a density of  $1.481 \text{ g cm}^{-3}$  [47]. Commercially available since 1964, it is the simplest, lowest cost and most widely used of the alkylsulfonic acids [48].

MSA occurs naturally in the sulfur cycle, forming in the atmosphere from the photochemical oxidation of dimethyl sulfide. Following deposition by precipitation, microbial degradation breaks MSA into sulfate and carbon dioxide [49]. It is a less toxic and environmentally friendly alternative to fluorosilicic and fluoroboric acids and has made these acids obsolete over the previous few decades in industrial applications such as the electroplating of lead alloys [46]. Furthermore, MSA is a non-oxidising acid that is less corrosive than sulfuric acid, which allows for easier, safer storage and transport as well as circulation through a flow circuit [48].

High electrolyte conductivity reduces energy loss in the cell. The ionic conductivity of MSA compares well with hydrochloric acid, at  $300 \text{ mS cm}^{-1}$  compared to  $346 \text{ mS cm}^{-1}$  for HCl, which is suitable for battery operation. Another favourable battery requirement is a high level of lead in the electrolyte. The saturation solubility of the lead methanesulfonate salt,  $Pb(CH_3SO_3)_2$ , in water is 2.6 M, which provides a sufficiently high storage capacity for battery operation. The solubility of lead methanesulfonate falls with increasing MSA concentration, from approximately 2.2 M at 0.9 M MSA, to almost zero near 8 M MSA. Beyond 2 M MSA, the solubility limit drops below 1.3 M, and the limit slightly increases with temperature [11]. In contrast, lead sulfate is insoluble in water and the solubility of lead chloride is also close to zero [46].

Lead and lead dioxide can also be deposited at high rates from aqueous MSA solutions, at  $60 \text{ mA cm}^{-2}$  [25] and  $100 \text{ mA cm}^{-2}$  [38] respectively. From Equation (11), this corresponds to a deposition

rate of  $3.4 \mu\text{m min}^{-1}$  for lead and  $7.9 \mu\text{m min}^{-1}$  for lead dioxide. In addition, studies by Velichenko *et al.* [38] have shown that the crystal structure of the deposits from MSA solutions are generally finer and more-oriented than those from acid nitrate solutions.

MSA is a well understood acid that has become very popular in electroplating applications. Because of this, its high conductivity, high metal salt solubility and overall safer nature, it is clear that MSA is the acid of choice for the soluble lead flow battery.

### **3.4 Electrolyte density and viscosity**

Work by Krishna *et al.* [50] has shown that there is a clear linear relationship between density and  $[\text{Pb}^{2+}]$ . Without free acid in the solution, the density increases from  $1.0 \text{ g cm}^{-3}$  at 0 M  $\text{Pb}^{2+}$  (pure water) to  $1.44 \text{ g cm}^{-3}$  at 1.5 M  $\text{Pb}^{2+}$ . When 1.0 M MSA is present in the solution, the density increases from  $1.03 \text{ g cm}^{-3}$  to  $1.48 \text{ g cm}^{-3}$  across the same  $[\text{Pb}^{2+}]$  range. The change in solution density when increasing [MSA] is relatively small, approximately  $0.05 \text{ g cm}^{-3}$  between 0 M and 1.5 M when  $[\text{Pb}^{2+}]$  is kept constant. This implies that during charge, as  $\text{Pb}^{2+}$  is removed from the electrolyte, the solution density will decrease overall despite the increase in acidity.

Because of its influence on density,  $[\text{Pb}^{2+}]$  has the dominant effect on viscosity, with values increasing by 130% as the  $\text{Pb}^{2+}$  concentration is increased from 0 M to 1.5 M whilst the MSA concentration is kept constant: the viscosity of 1 M MSA solution is  $1.12 \text{ mPa s}$  whilst this increases to  $2.61 \text{ mPa s}$  in 1.5 M  $\text{Pb}^{2+}$ . During charge of the soluble lead battery, [MSA] increases at twice the rate of the decrease in  $[\text{Pb}^{2+}]$ . Despite this, the overall electrolyte viscosity will decrease. Conversely, viscosity will increase during battery discharge.

### **3.5 Electrolyte conductivity**

Further work by Krishna *et al.* established a more complicated relationship between electrolyte composition and ionic conductivity. The conductivity increases with increasing [MSA] when  $[\text{Pb}^{2+}]$  is held constant. As a function of  $[\text{Pb}^{2+}]$  however, the conductivity follows a different relationship: at  $\leq 0.25$  M MSA, conductivity increases with  $[\text{Pb}^{2+}]$ ; at  $\geq 1.0$  M MSA it decreases with increasing  $[\text{Pb}^{2+}]$ ; between MSA concentrations of 0.25 M and 1.0 M, it peaks at approximately 0.75 M  $\text{Pb}^{2+}$ . This behaviour is likely due to the complexing behaviour of the methanesulfonate anion to the  $\text{Pb}^{2+}$  cation and changes in the overall solution viscosity affecting the ionic mobility of the charged species.

A solution of 1.5 M  $\text{Pb}^{2+}$  and 1.0 M MSA has a conductivity of  $220 \text{ mS cm}^{-1}$  at 298 K. This is comparable to electrolytes used in the all-vanadium flow battery: an anolyte containing 1.5 M of  $\text{V}^{3+}$  and 4 M  $\text{H}_2\text{SO}_4$  has an electrolytic conductivity of  $187.6 \text{ mS cm}^{-1}$ , whilst a catholyte of 1.5 M  $\text{V}^{4+}$  and 4 M  $\text{H}_2\text{SO}_4$  has a value of  $294.8 \text{ mS cm}^{-1}$ , both at 298 K [51].

## 4 Electrode kinetics

### 4.1 Negative redox couple

Cyclic voltammetry was carried out by Wallis and Wills [14] separately for each redox couple in order to understand the electron transfer kinetics and reversibility of both electrode reactions. The  $\text{Pb}^{2+}/\text{Pb}$  couple at the negative electrode was investigated using a three-electrode glass cell with  $25 \text{ cm}^3$  of electrolyte. A glassy carbon rotating disc electrode (RDE) set at 900 rpm was placed in a solution of 10 mM  $\text{Pb}^{2+}$  and 1.5 M MSA. A platinum wire was used as the counter electrode and potentials were measured against a saturated calomel reference electrode (SCE). All potentials in the following section are stated versus SCE. The potential was cycled 200 times between -0.2 V and -0.7 V. The 1st and 200th cycle are superimposed in Figure 3.

Sweeping negatively from -0.2 V, a cathodic reduction wave is seen at -0.55 V, reaching a limiting current density of  $-5 \text{ mA cm}^{-2}$ . This suggests the nucleation and deposition of a solid metal species. On the reverse scan from -0.7 V, reduction continues until -0.48 V, at which point an anodic oxidation curve begins, later peaking at -0.39 V before sharply decreasing. This represents the dissolution of the deposit back into solution. The entire voltammogram is characteristic of the deposition and subsequent dissolution of a  $M^{2+}/M$  couple, where the kinetics are rapid and the overpotentials are low. There is little change in the voltammogram shape after 200 cycles, suggesting that this is a highly efficient and repeatable process.

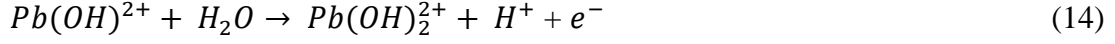
In a similar study showing similar voltammogram profiles [11], the charge efficiency was calculated to be close to 100%. No substantial hydrogen evolution was observed, and this result held true under a variety of electrode materials (glassy carbon, gold, platinum) and electrolyte concentrations (1 - 300 mM  $Pb^{2+}$  and 0.1 - 5 M MSA), with only minor differences in the peak potentials.

### FIGURE 3 NEAR HERE

## 4.2 Positive redox couple

According to data from Fleischmann *et al.* [52], the oxidation of dissolved  $Pb^{2+}$  species in solution and the subsequent deposition of  $PbO_2$  at an anode surface is a two-electron transfer process, which occurs over two stages. The mechanism is irrespective of the solution, which only affects the deposition rate. This was further explored by Velichenko *et al.* [38], who suggest the following mechanism:





H<sub>2</sub>O is oxidised at the anode surface, splitting into H<sup>+</sup> and the ·OH radical, which adsorbs onto the electrode surface. This interacts with a Pb<sup>2+</sup> ion, forming soluble Pb(OH)<sup>2+</sup>. Following the second oxidation step, a soluble Pb<sup>4+</sup> compound, Pb(OH)<sub>2</sub><sup>2+</sup> accumulates near the electrode surface. This molecule then decomposes into PbO<sub>2</sub>, which crystallises on the electrode surface.

Velichenko *et al.* investigated this mechanism in methanesulfonic and nitric acid media and the process remained the same in both cases. However, the rate of deposition was found to be greater in the presence of methanesulfonate.

Cyclic voltammetry of the Pb<sup>2+</sup>/PbO<sub>2</sub> couple at the positive electrode was also investigated by Wallis and Wills [14]. A solution of 0.5 M Pb<sup>2+</sup> and 1.5 M MSA was used and the set-up remained the same as that for the negative voltammetry test. The potential was swept between 0.2 V and 1.9 V for 100 consecutive cycles. The 1st and 100th cycles are presented together in Figure 4.

Sweeping positively, deposition of PbO<sub>2</sub> in the 1st cycle is seen to commence at 1.8 V. PbO<sub>2</sub> deposition continues on the backward scan, from 1.9 V until 1.45 V, suggesting that the deposition of PbO<sub>2</sub> onto layers of PbO<sub>2</sub> is kinetically more facile than onto a glassy carbon substrate. A similar deduction for Pb deposition can be made from the negative electrode voltammogram.

Continuing the potential sweep negatively from 1.5 V leads to a well-defined cathodic reduction peak between 1.2 V and 0.95 V, reaching a current density of  $-200 \text{ mA cm}^{-2}$ . It is clear that  $\text{PbO}_2$  is being deposited and later stripped back into solution. The electron transfer kinetics are considerably slower than the  $\text{Pb}^{2+}/\text{Pb}$  couple, as seen by the large separation in potential between the oxidation and reduction peaks.

Whilst the deposition of  $\text{PbO}_2$  takes place at high current densities at negatively shifted potentials in the cycles after the first, the stripping region is seen to broaden and the peak current density decrease. By the 100<sup>th</sup> cycle, the stripping region ranges from 1.4 V to 0.2 V, peaking at just  $-75 \text{ mA cm}^{-2}$ . This puts into perspective the difficulty of reducing layers of  $\text{PbO}_2$ , which leads to the gradual accumulation of the deposit with each cycle.

These results suggest that in a cell under operation, the accumulation of  $\text{PbO}_2$  at the positive electrode would result in an accumulation of Pb at the negative. By improving the kinetics at the positive electrode, the negative electrode would therefore also benefit.

## **FIGURE 4 NEAR HERE**

## **5 Operating conditions**

### **5.1 Negative electrode**

To maximise the cell performance and lifetime, deposition on charge must be uniform across each electrode surface. The deposits should be smooth, compact and well-adhered whilst also remaining

easy to dissolve on discharge. The morphology and other properties of the deposits will depend on the operating conditions, such as the temperature, current density, flow rate and electrolyte composition in terms of  $[Pb^{2+}]$  and  $[MSA]$ .

Lead coatings are used for corrosion resistance of the base metal, particularly if the material is to come into contact with sulfuric acid; the surface of the lead forms a passivating sulfate layer that protects the layers within. To ensure material integrity, the coating must be devoid of pits and cracks. Typically, coatings up to 0.2 mm are deposited [25], whereas the target for SLFB operation is often reported to be 1 mm [31].

In the absence of a suitable surfactant the formation of large crystals, referred to as dendrites, can be seen across the cathode surface. In particular, dendrites can grow rapidly along the internal cell walls at the edges of the electrodes, using the non-conducting surface as a scaffold (not to be mistaken with 'edge effects' that occur at non-parallel plate electrodes, such as the rotating disc electrode [53]).

Dendrites, and other rocky forms of growth, can short the cell and are more susceptible to being dislodged by the electrolyte flow. The current density is highest where the distance between the negative and positive electrodes is lowest [53]. Hence, any slight growth of lead towards the positive electrode will result in an increase in the current density in that area, resulting in a greater deposition rate; the further the tip of the growth is from the cathode surface, the faster it grows in size. This positive feedback loop allows Pb dendrites to form rapidly, stressing the importance of uniform, smooth deposition at all times. In addition, high temperatures lead to coarser grain sizes, which would exacerbate this mechanism. In industry, the lead plating bath temperature is controlled between 293 K and 313 K [25].  $PbO_2$  is far less conductive than Pb, which is why it is not possible to produce  $PbO_2$  dendrites as the rate of electron transfer is slow.



Additives must be used in order to produce compact, smooth deposits and many organic surfactants are used routinely in industry. They work by inhibiting the deposition process; the rate of deposition can therefore be controlled by selecting the concentration of the additive. Studies by Pletcher *et al.* [31] trialled over 30 additives in lead deposition experiments focusing on stirred MSA baths. Two additives stood out for their ability to produce good quality lead deposits: lignosulfonate (as the sodium salt, or lignosulfonic acid) [15] and hexadecyltrimethylammonium hydroxide (HDTMA) [31].

Their experiments also investigated other conditions affecting deposition quality. In Figure 5, four SEM images display the effect of increasing  $[Pb^{2+}]$  and current density at ambient temperature on the deposit morphology. Deposition time was 2 hrs, and the substrate material was carbon/high density polyethylene (C-HDPE), with a scraped nickel surface (Section 7), An unstirred Hull cell was used for each test [31].

## FIGURE 5 NEAR HERE

Images (a) and (b) show samples deposited from a solution composed of 0.5 M  $Pb^{2+}$  and 1.0 M MSA, with 5 mM HDTMA. Images (c) and (d) used the same MSA and HDTMA concentration, but  $[Pb^{2+}]$  was increased to 1.5 M. Furthermore, images (a) and (c) were deposited using a current density of  $25 \text{ mA cm}^{-2}$ , whilst images (b) and (d) used  $50 \text{ mA cm}^{-2}$ .

Image (a) shows the smoothest produced deposit. Compact, circular grains of equal size with few voids in between can be seen, and there are no protrusions from the surface. When the current density

is increased to  $50 \text{ mA cm}^{-2}$  in image (b), larger grains up to  $200 \mu\text{m}$  in width are formed and several protrusions can be seen. The grains now vary in size and the surface appears rougher. However, the grain orientation is relatively ordered.

At higher  $[\text{Pb}^{2+}]$ , the deposit is markedly different: image (c) consists of a variety of grain sizes with numerous pores across the surface. There are many protrusions and the grains are more randomly orientated. When the current density is increased to  $50 \text{ mA cm}^{-2}$  in image (d), there is little to no preference in grain orientation. Grain size varies from as small as those seen in image (a) to extremely large, dendritic structures that rise high above the deposit surface.

Several tests were also conducted varying the HDTMA concentration. There was little difference to the morphology (a) when zero additive was used. However, the grains in image (b) were less refined and more varied in shape in the absence of HDTMA, creating a rougher surface. When test (c) was repeated with  $20 \text{ mM}$  HDMTA, the deposit was improved, appearing more uniform and compact than image (b) but not as fine as image (a). Test (d) was also repeated with the higher HDTMA level, and the improvement was even greater than that seen for test (c). Though the grain orientation is unaffected, the larger crystals were subdued and there was greater uniformity across the surface. Furthermore, the deposits were also visibly more reflective. If the SLFB is to contain a high  $\text{Pb}^{2+}$  concentration and is charged at high current densities, then a high concentration of HDTMA becomes necessary to ensure reliable deposition.

The effect of increasing  $[\text{MSA}]$  was also studied, and the results can be seen in Figure 6.

**FIGURE 6 NEAR HERE**

Images (a) and (b) show SEM images of samples deposited from a solution containing 0.3 M  $\text{Pb}^{2+}$  and 1.0 M MSA, with 5 mM HDTMA. Images (c) and (d) use the same  $\text{Pb}^{2+}$  and HDTMA concentration, but [MSA] is increased to 2.4 M. In addition, images (a) and (c) were deposited under a current density of  $25 \text{ mA cm}^{-2}$ , whilst images (b) and (d) used  $50 \text{ mA cm}^{-2}$ .

There does not seem to be significantly more void areas in image (c) compared to (a). Whilst (a) appears to be very smooth with tightly packed grains, (c) appears to have elevated regions, each consisting of a cluster of grains. This differs from the images in Figure 5, where any protrusion was seen to be of a single grain.

As seen in image (d), the greater level of MSA and the high current density results in rocky, dendritic clusters scattered randomly across the deposit surface, with randomly oriented, moderately sized grains forming the base layer. The authors therefore suggest that [MSA] in SLFB electrolytes should not exceed a limit of 2 M MSA [31].

Finally, it was found that time is also an important factor in determining the quality of the deposit. As deposition time wore on, the deposit quality from all electrolyte compositions was seen to tend towards Figure 5d or 6d, depending on  $[\text{Pb}^{2+}]$  and [MSA].

## 5.2 Positive electrode

It is possible to deposit pure  $\alpha$ - or pure  $\beta$ - $\text{PbO}_2$ , as well as a mixture of both phases. However, the deposition conditions from aqueous solutions required to accurately achieve a certain purity of either phase is still inconclusive. It was believed that the  $\alpha$ -phase is deposited from high pH solutions, whereas the  $\beta$  phase is favoured under acidic conditions [41]; studies regarding MSA-based solutions

by Pletcher *et al.* [32], Li. *et al.* [33], Sirés *et al.* [54] and Velichenko *et al.* [38] showed that this is not always the case. The phase and morphology depend on the electrolyte composition and temperature, the substrate material, the rate of deposition and the deposit thickness, in addition to repeated deposition and stripping during battery operation.

Pletcher *et al.* [32] studied the deposition of  $\text{PbO}_2$  onto C-HDPE electrodes from stirred MSA solutions. It was found that compact, well-adhering layers up to 1 mm could be deposited under a variety of electrolytes, with  $[\text{Pb}^{2+}]$  and  $[\text{MSA}]$  ranging from 0.1 - 1.5 M and 0 - 2.4 M, respectively, and with 5 mM HDTMA in solution. Higher current density was seen to create more compact deposits. Figure 7 presents a selection of SEM images where certain deposit defects can be seen.

## FIGURE 7 NEAR HERE

Images (a) and (c) present SEM images of a  $\text{PbO}_2$  surface deposited from a solution containing 0.5 M  $\text{Pb}^{2+}$  and 0.3 M MSA, with 5 mM HDTMA (stirred solution 500 rpm, parallel-plate beaker cell). Images (b) and (d) use the same HDTMA concentration, but  $[\text{Pb}^{2+}]$  and  $[\text{MSA}]$  are both increased to 1.5 M (unstirred Hull cell). Regarding the deposition rate, images (a) and (d) were deposited at  $50 \text{ mA cm}^{-2}$ , whilst images (b) and (c) used  $20 \text{ mA cm}^{-2}$  and  $150 \text{ mA cm}^{-2}$  respectively.

In general, the deposits appear smooth at all three scales of magnification, from  $1000 \mu\text{m}$  in image (c), to  $500 \mu\text{m}$  in image (a), to  $100 \mu\text{m}$  in images (b) and (d), with round grains of uniform size and no voids in between. There is little difference between the deposits, despite the wide range of current density, concentration of  $[\text{Pb}^{2+}]$  and  $[\text{MSA}]$ , and the fact that (a) and (c) were deposited under stirred

conditions whilst (b) and (d) from static conditions. There are two other notable observations.

In the  $150 \text{ mA cm}^{-2}$  deposition seen in image (c), the black spots indicate damage caused by oxygen evolution. The current density at which gassing occurred was seen to decrease with decreasing  $[\text{Pb}^{2+}]$  and increasing [MSA]. For example, in another study that used a solution of  $0.3 \text{ M Pb}^{2+}$  and  $2.4 \text{ M MSA}$ , oxygen evolution was observed at  $50 \text{ mA cm}^{-2}$ . This was also confirmed by Velichenko *et al.* [38], where it is suggested that high [MSA] inhibits  $\text{PbO}_2$  deposition due to excessive complexation.

In image (d), a large fissure is seen running across the centre of the image. This is not seen in image (b), which used the same electrolyte but was deposited at  $20 \text{ mA cm}^{-2}$ . It is suggested that at a high MSA concentration of  $1.5 \text{ M}$  and a high current density of  $50 \text{ mA cm}^{-2}$ , the compact deposit becomes stressed, leading to cracks at the deposit surface. In a flow battery, this would likely result in the breaking away of layers into the electrolyte. The conditions during operation therefore must be carefully controlled to avoid such losses in energy capacity [32].

Voltammograms conducted by Li *et al.* [33] studied further the consequences of thick  $\text{PbO}_2$  deposits. On reduction, thicker deposits were seen to increase the overpotential, shifting the reduction potential to more negative values whilst broadening the reduction peak. The difficulty of this mechanism appears to be the main impediment to further SLFB development, and it is attributed to an insufficient supply of protons to the inner layers of the  $\text{PbO}_2$  deposit (Section 5.5).

In further morphology studies, Li *et al.* saw a correlation between  $\alpha\text{-PbO}_2$  and smooth deposits. In addition, whilst both phases were seen to form compact deposits, it was suggested that the presence of  $\beta$  layers amongst the  $\alpha$  layers could be a precondition leading to powdery deposits. Temperature was discovered to be the most influential parameter on determining the phase:  $\alpha$  deposits were

favoured at lower temperatures, producing pure  $\alpha$ -PbO<sub>2</sub> at 298K. Pure  $\beta$ -PbO<sub>2</sub> was deposited between 333 K and 348 K, and a mixture of both phases occurred between 298 K and 333 K. The mean grain size was also seen to grow, from 18 nm at 298 K to 57 nm at 348 K.

Deposition under mass transport control also resulted in the deposition of the  $\beta$  phase. The deposit is also powdery and poorly-adhering. A higher [Pb<sup>2+</sup>], at least above 0.3 M, was seen to deposit  $\alpha$ - as the dominant phase. In a charge/discharge study using a stirred beaker cell filled with 0.5 M Pb<sup>2+</sup> and 0.5 M MSA, at 298 K, the PbO<sub>2</sub> deposit was seen to accumulate and become rougher with each cycle; the early cycles deposited a majority  $\alpha$ -PbO<sub>2</sub> deposit, with the proportion of  $\beta$ - structures growing with each following cycle.

The proportion of  $\alpha$ -PbO<sub>2</sub> in the LAB is also seen to decrease with cycling. The positive active mass is prepared by mixing lead oxide (PbO) with other components. After curing, the electrode is oxidised in a cell to form PbO<sub>2</sub> (known as the Planté formation process). In experiments reported by Yeh *et al.* [55], one of these electrodes contained 13.9% and 82.0% of the  $\alpha$ - and  $\beta$ - phase respectively. Following 100 charge/discharge cycles, the proportions were seen to reduce to 8.8% and 81.7% respectively (with the proportion of PbSO<sub>4</sub> increasing).

Sirés *et al.* [54] are largely in agreement with Pletcher *et al.* and Li *et al.* Whilst temperature shows the greatest influence on phase, low [MSA] and high [Pb<sup>2+</sup>] are required to avoid extremely porous deposits riddled with many cracks and voids. Defects such as these result in a poorly-adhering, powdery deposit.

### **5.3 Further discussion on the structure of lead dioxide**

The discussion so far has assumed a stoichiometric PbO<sub>2</sub> deposit. However, it is known that both  $\alpha$ -

and  $\beta$ - structures instead exist as  $\text{PbO}_x$ , where  $1.85 < x < 2.05$  in the LAB [56].  $\text{H}_2\text{O}$  is also widespread inside the pores. The theory proposed by Rüetschi [57] and backed up by experimental data, suggests that there are cation vacancies separating ordered, crystal zones within the lattice.  $\text{Pb}^{2+}$  ions could occupy these vacancies, leading to a structure proposed as  $(\text{Pb}^{4+})_{1-x-y}(\text{Pb}^{2+})_y(\text{O}^{2-})_{2-4x-2y}(\text{OH}^-)_{4x+2y}$  where  $x$  and  $y$  are the number of vacant cation sites and incorporated  $\text{Pb}^{2+}$  ions, respectively as a fraction of the overall number of cation sites (i.e. involving those occupied by  $\text{Pb}^{4+}$  as well).

Dopant cations can also occupy these vacant positions, affecting the properties and the ratio of  $\alpha$ - and  $\beta$ - structures [58]. For example, large cations such as bismuth are reported to promote  $\alpha$  growth [59].

Such lattice defects lead to conductive properties.  $\text{PbO}_2$  therefore is regarded as an n-type semiconductor [18], but  $\beta$ - $\text{PbO}_2$  has also been considered as a semi-metal [60]. Despite  $\alpha$ - $\text{PbO}_2$  having a more compact structure, there is greater ionic mobility in  $\beta$ - $\text{PbO}_2$ . The conductivity of the latter is therefore higher, at the  $10^4 \text{ S cm}^{-1}$  scale compared to the  $10^3 \text{ S cm}^{-1}$  scale of the former [42].

In the LAB, the compactness of  $\alpha$  structures provides mechanical stability with the current collector grid, but this also makes it more difficult to discharge (i.e. reduce to  $\text{PbSO}_4$ ) [61]. In contrast, the  $\beta$  structures offer a greater energy storage capacity and can be discharged at higher current densities, but the susceptibility for active mass shedding is greater [62]. The balance between LAB performance, charge capacity and lifetime depends on the ratio of  $\alpha$ - and  $\beta$ - $\text{PbO}_2$  within the positive active mass, amongst other factors [56]. The former provides integrity by acting as a binding agent, whilst the latter provides the electrochemical performance. It is claimed by Kiessling [62] that during cycling, the proportion of  $\alpha$ - $\text{PbO}_2$  and  $\beta$ - $\text{PbO}_2$  decreases and increases respectively, until an equilibrium is reached at 20% and 80%, respectively.

## 5.4 Potential–time plots

In order to continue the discussion on lead dioxide, it is useful to first understand the shape of a potential-time response during a galvanostatic charge/discharge cycling experiment of a soluble lead flow cell. Figure 8 presents a typical result. The 100 cm<sup>2</sup> sized positive and negative electrodes were composed of a 2D carbon polymer surface, with impregnated RVC fragments (Section 7). The electrolyte consisted of 1 dm<sup>3</sup> 1.5 M Pb<sup>2+</sup> and 1.0 M MSA, with 1 g dm<sup>-3</sup> lignosulfonic acid, this being circulated past the electrodes in the undivided cell at 2.5 cm s<sup>-1</sup>. The cell was operated throughout at 20 mA cm<sup>-2</sup> [17].

9 cycles are presented overall. The first 6 cycles each consist of a 15 mins charge followed by a discharge to 1.2 V (or for a maximum of 15 min). In the subsequent 3 cycles, the charge/max discharge time is increased to 60 min. The potentials of the individual electrodes vs. SCE, E<sub>+</sub> and E<sub>-</sub>, are presented alongside the overall cell potential,  $U_{cell}$ , providing insight as to which electrode limits the overall cell potential during operation.

### FIGURE 8 NEAR HERE

The charge and discharge potentials of the negative electrode are close to -0.5 V and -0.3 V respectively, approximately corresponding to the deposition and stripping potentials seen in the cyclic voltammetry of the Pb<sup>2+</sup>/Pb couple (Section 4.1). The potentials are generally constant and stable throughout the experiment, particularly in the later cycles.

In contrast, the positive potentials are more complicated. The discharge potential is flat in the 1st



cycle, at 1.25 V, before starting to decrease from 1.25 V in each consecutive discharge phase. The charge potential is stable only for the 1st cycle, at 1.6 V. In all other cycles, the charge potential starts at lower potentials ( $1.5 < E^+ < 1.6$  V) after an initial spike, before instantly dropping to  $\leq 1.5$  V, and finally rising again to 1.6 V later on. The gap between the upper and lower potential is clearer in the latter cycles, where over half the charge phase takes place at the lower potential.

In the 1st cycle, the negative potential rises sharply towards the end of discharge, which causes the cell potential to drop to 1.2 V. This voltage spike decreases in size with each following cycle, finally becoming flat in the 5th cycle. During this time, the limiting electrode on discharge transitions from the negative to the positive. The shape of the positive electrode's potential-time response is discussed further in the following section.

## 5.5 Discharge at the positive electrode

Section 5.4 introduced a potential-time response of a cycling experiment involving a soluble lead flow cell, where the positive electrode potential on charge appears to follow a complex pattern. There is an initial potential spike at the start of charge that is likely due to a high nucleation overpotential, followed by a dip in potential that subsequently increases later on during the charge phase.

The voltage dip on charge could be explained by the properties of  $\text{PbO}_x$ , where  $x$  could have a value as low as unity.  $\text{PbO}$  could be formed during the discharge phase of the previous cycle. EDAX analysis conducted by Pletcher and Wills [30] identified the presence of  $\text{PbO}$  after several charge/discharge cycles in a separate cycling experiment.

Over the charge phase of the first cycle in Figure 8, only  $\text{Pb}^{2+}$  is oxidised to a near-stoichiometric  $\text{PbO}_2$  deposit, resulting in a constant charge potential. It was seen in Section 4.2 that the

deposition/dissolution mechanism of  $\text{PbO}_2$  is a complex, multi-stage procedure. During discharge, high  $[\text{Pb}^{2+}]$  exceeding the solubility limit near the deposit surface, in addition to low  $[\text{H}^+]$  near the surface or within the pores, could lead to the formation of  $\text{PbO}$  [30], or perhaps a low value of  $x$  in  $\text{PbO}_x$ . Proton starvation would result in a relatively high local pH. This condition could be created if the  $\text{PbO}_2$  deposit becomes very compact, i.e. a large  $\alpha\text{-PbO}_2$  presence. The formation of  $\text{PbO}$  could then be facilitated as predicted by the potential-pH diagram for the lead-water system [44].

In the following cycle's charge phase,  $\text{PbO/PbO}_x$  would be preferentially oxidised to  $\text{PbO}_2$ , resulting in the lower potential. Once all the conductive  $\text{PbO}_x$  has been oxidised, normal oxidation of  $\text{Pb}^{2+}$  into  $\text{PbO}_2$  is resumed and the potential returns to its higher level. Because this charge profile is seen in every cycle but the first, it can be assumed that the rate of  $\text{PbO/PbO}_x$  formation during the discharge phase is equal to or greater than the rate of oxidation of  $\text{PbO/PbO}_x$  into  $\text{PbO}_2$  on charge, or that there is a proportion of  $\text{PbO/PbO}_x$  that remains insoluble. As  $x$  reduces from 2 to 1, its conductivity also drops. Certain  $\text{PbO}_x$  compounds therefore could remain insoluble. Described by Oury *et al.* [63] as a 'passivating' layer within the deposit, this could cause the accumulation of the  $\text{PbO}_2$  deposit with each cycle by preventing the thorough dissolution of the overall deposit.  $\text{H}^+$  is required to instigate the dissolution mechanism. With a high MSA bulk electrolyte concentration, Oury *et al.* suggest that  $\text{H}^+$  can penetrate deep into the deposit and reduce the inner layers to passivating  $\text{PbO}_x$  compounds, creating an insulating layer between the electrode and the outer  $\text{PbO}_2$  layers, preventing the dissolution of these outer layers. With a low MSA bulk electrolyte concentration,  $\text{PbO}_x$  formation is restricted to isolated clusters on the deposit surface, which can then be further reduced during discharge, or oxidised to near stoichiometric  $\text{PbO}_2$  during charge.

This theory appears to disagree with that of Pletcher and Wills [30], who suggested that low  $[\text{H}^+]$  near the electrode surface instead of high  $[\text{H}^+]$  contributes to  $\text{PbO}$  formation, although a number of other

factors are suggested. Regardless, previous claims that  $\alpha$ -PbO<sub>2</sub> is better suited to the SLFB [33] are premature and a deeper understanding of PbO<sub>2</sub> stripping and deposition is required. Whilst forming a compact deposit is favourable for energy capacity and cell design in the SLFB, this same property makes  $\alpha$ -PbO<sub>2</sub> more likely to suffer from surface cracks (Section 5.2). Furthermore, the compactness could also lead to a lack of protons inside the pores making it difficult to reduce on discharge. This difficulty is also seen in the LAB;  $\beta$ -PbO<sub>2</sub> is more conductive but tends to form powdery deposits that are prone to flaking from the electrode surface (Section 5.3). A better understanding of the PbO<sub>2</sub> deposit formed in the SLFB during cycling is needed along with further comparisons to the LAB, as it is likely that a certain ratio of  $\alpha$  to  $\beta$ -PbO<sub>2</sub> is required to improve the performance and cycle life of the SLFB.

Verde *et al.* [37] experimented with potentiostatic deposition using a stirred beaker cell with graphite electrodes. Charging at 1.8 V, the current-time transient settled close to 7 mA cm<sup>-2</sup>, producing 41%  $\alpha$  and 59%  $\beta$ -PbO<sub>2</sub> after 60 mins. In contrast, under the same conditions at 1.9 V, the transient averaged 16 mA cm<sup>-2</sup> and the ratio shifted to 97%  $\alpha$ - and 3%  $\beta$ -PbO<sub>2</sub>.

Higher voltage was also seen to promote nanoparticle PbO<sub>2</sub> growth whilst larger particles were produced at 1.8 V. Following galvanostatic discharging at 20 mA cm<sup>-2</sup>, the deposit that had been produced at 2.0 V was seen to offer almost twice as much capacity as that deposited at 1.8 V, where much of the deposit remained on the electrode. Verde *et al.* therefore place great emphasis on the PbO<sub>2</sub> deposit grain size.

## **5.6 Further observations at the positive electrode**

A powdery deposit, or one that is cracked at the surface, is poorly-adhering and is more prone to breaking away from the electrode. Insoluble particles of PbO<sub>2</sub> stuck in the flow circuit or in the

electrolyte reservoir have been seen in several SLFB studies [16, 17, 34]. This poses two problems: firstly, energy capacity is lost as these particles cannot be dissolved electrochemically.  $[\text{Pb}^{2+}]$  in solution is therefore decreased, which affects the deposition quality during subsequent charging. Secondly, if not filtered out,  $\text{PbO}_2$  particles can restrict or block the electrolyte flow and damage the pump. Additionally, the amalgamation of these particles can lead to a gel-like, black, insoluble sludge [17]. The sludge is soft and can collect in areas which are stagnant or which see low flow velocity, as well as damaging the positive electrode by forming a thin film over it.

Additionally, Wills *et al.* [17] reported the 'creep' of  $\text{PbO}_2$  deposits along the cell wall and inlet/outlet flow distributor, adhering strongly to the non-conductive polymer surfaces which were seen to act as a scaffold. These were difficult to dissolve on discharge and contributed to cell shorting. These various failure mechanisms are illustrated in Figure 9.

## FIGURE 9 NEAR HERE

A strategy for re-dissolving Pb and  $\text{PbO}_2$  deposits remaining on the electrode and cell wall, and solid particles in solution has been proposed by Collins *et al.* [34], and this is discussed in Section 10.2.

### 5.7 Flow rate

A high flow rate providing uniform mass transport of active species to the entire electrode surface, and removal of products including gas bubbles from the electrode surface (especially at high current densities), will ensure a uniform current distribution across the electrode. Secondary reactions will be minimised and the uniform flux of  $\text{Pb}^{2+}$  to the electrode surfaces will ensure well-adhered, uniform deposits [53]. This is continued in relation to 3D RVC electrodes in Section 7.

There is little work regarding the flow rate in the soluble lead flow battery. Understanding the relationship between flow rate and cell performance is important, as this could minimise the pump power whilst maintaining good electrochemical performance. The flow rate was briefly explored by Pletcher and Wills [30], where little difference in performance of a small flow cell with 2 cm<sup>2</sup> electrodes was seen between 2 and 10 cm s<sup>-1</sup>. These studies were carried out at a current density of 20 mA cm<sup>-2</sup> and a high [Pb<sup>2+</sup>] of 1.5 M. Control of the flow rate becomes more important at higher current densities and at higher states of charge, where there is lower [Pb<sup>2+</sup>] in solution.

Verde *et al.* [37] explored flow rates in the form of a stirred beaker cell using 2.5 cm x 3.5 cm electrodes with a ¼" separation in 140 ml of electrolyte. Galvanostatic charge at slow stir rates resulted in larger PbO<sub>2</sub> particle formation, which were seen to produce deposits that were difficult to reduce on discharge. A high stir rate of 700 rpm was critical to ensure a PbO<sub>2</sub> deposit composed of smaller particles, which led to the cell achieving 2000 cycles at 79% energy efficiency (20 mA cm<sup>-2</sup>, 60 mins galvanostatic cycling). However, the flow distribution and flow dynamics cannot be extrapolated without further details of the experiment (dimensions of the beaker and stirrer bar etc.). Equivalent data should be obtained in a flow cell.

## **6 Additives**

### **6.1 Negative electrode**

The need for additives to inhibit the rate of lead deposition and produce non-dendritic, uniform, smooth deposits was introduced in Section 5.1. Pletcher *et al.* [31] studied a comprehensive set of additives for the negative electrode, and two additives were selected and subsequently used in flow cell experiments. These were sodium lignosulfonate or lignosulfonic acid, at a preferred concentration

of  $1 \text{ g dm}^{-3}$  and hexadecyltrimethylammonium hydroxide (HDTMA),  $\text{CH}_3(\text{CH}_2)_{15}\text{N}(\text{OH})(\text{CH}_3)_3$ , preferred at 5 mM. The preferred average molecular weight of the lignosulfonate is not reported.

Lignin, a naturally occurring polymer found in wood, can be sulfonated to form lignosulfonate. It is a macromolecule with a complex structure based around the bonds between phenylpropane groups, with micropores in between. When adsorbed onto an electrode, these micropores allow the movement of ions through the structure. It is used as part of an 'expander' in the LAB, creating a porous  $\text{PbSO}_4$  layer and preventing the formation of an insulating sulfate layer on discharge [18].

Whilst dendrite-free, compact deposits were produced, electrochemical studies showed that lignosulfonate adversely affects the overpotentials and charge efficiency at both electrodes, leading to a lower overall energy efficiency in flow cell cycling [15]. In addition, the amber colour of the electrolyte, due to the lignosulfonate, was seen to fade during these tests. It is likely that these molecules are oxidised at the positive electrode, potentially affecting the additive's ability to control the quality of the lead deposit. However, the relation between discolouration and cell performance is not clearly seen in the results.

Pletcher et al. place HDTMA in the same high 'lead deposit quality' category as lignosulfonate but a direct comparison as to which additive produces better deposits is not discussed. Unlike the latter, HDTMA was not seen to adversely affect the positive electrode reaction or affect the overpotential at either electrode. Additionally, it is considerably more expensive than lignosulfonate [47]. Both additives have been tested in short term flow cell studies, but the long term stability at elevated temperatures has not yet been investigated.

## 6.2 Positive electrode

Lead dioxide coatings can be doped with both metallic and non-metallic ions in order to enhance a certain property of the coating. This has been reviewed by Li *et al.* [41], where lead dioxide composites, i.e. those containing solid particles such as other metal oxides, are also discussed. Bismuth cations,  $\text{Bi}^{3+}$ , are known to improve the ability of the coating to oxidise inorganic ions [64] whereas fluoride ion,  $\text{F}^-$ , is known to improve the adhesion of the coating to the substrate [65] whilst inhibiting oxygen evolution [66].

Wallis and Wills [14] investigated the use of bismuth in the soluble lead system. Through cyclic voltammetry,  $\text{Bi}^{3+}$  was seen to improve the kinetics of the  $\text{Pb}^{2+}/\text{PbO}_2$  couple, shifting the stripping peak in later cycles to more positive potentials whilst preventing the broadening of the stripping region. However, similar experiments showed the  $\text{Bi}^{3+}/\text{Bi}$  deposition potential from MSA solution to be more positive than that of  $\text{Pb}^{2+}/\text{Pb}$ , suggesting that in a flow cell, bismuth would be preferentially deposited at the negative electrode before the lead, or forming an alloy. Wallis and Wills also report a series of charge/discharge experiments using a soluble lead cell with static electrolytes. In order to avoid depletion of  $\text{Bi}^{3+}$  from the electrolyte through deposition at the negative electrode, a separator is introduced to confine  $\text{Bi}^{3+}$  to the positive half-cell. The cell lifetime was seen to increase in this configuration, and this remains to be tested in larger cells using flowing electrolytes.

Chen *et al.* [59] have studied the use of bismuth in the LAB. Doping lead oxide with  $\text{Bi}^{3+}$  promotes the growth of the more-compact  $\alpha\text{-PbO}_2$  phase during formation, yet also making the  $\text{PbO}_2$  active material more porous. Together, this has the effect of improving battery capacity and lifetime. The pore-creating ability of bismuth therefore could be useful in the soluble lead system, where a compact  $\text{PbO}_2$  deposit was attributed to the difficulty in reducing the deposit (Section 5.5).

Oury *et al.* [67] have trialled fluoride containing electrolytes in flow cell cycling tests. In the presence

of the preferred concentration of 60 mM, the amount of powdery lead dioxide particles in the electrolyte reservoir (dislodged from the positive electrode) was substantially reduced. The lead dioxide adhesion to the electrode had improved without any detrimental impact on the reaction kinetics at either electrode.

Whilst other additives such as  $\text{Fe}^{3+}$  and  $\text{Ni}^{2+}$  have been tested for use in the SLFB [15], only  $\text{Bi}^{3+}$  and  $\text{F}^-$  are reported in the literature for successfully improving the positive electrode reactions during cell cycling. A more comprehensive investigation is needed to identify further additives, and combinations of additives, that could enhance the reversibility of the  $\text{Pb}^{2+}/\text{PbO}_2$  reaction.

## **7 Electrode materials**

Lead coatings are deposited onto metals such as steel for protection from corrosive, mainly sulfuric acid-containing media [25], whereas lead dioxide coatings are commonly deposited onto a lead/lead alloy, carbon, or titanium substrate depending on the application [41]. Since the 1970s, flow battery research and manufacture had sought to employ inexpensive electrodes with high electrical conductivity and chemical stability. Carbon based materials satisfy these requirements and have been widely used in a number of flow battery systems, including all- vanadium, zinc-bromine and soluble lead [66].

2D electrodes refer to an electrode with a flat surface, such as a carbon polymer electrode. 3D electrodes, such as reticulated vitreous (glassy) carbon, meshes and felts, exist as a matrix through which the electrolyte can flow past or through. These can be attached through heat bonding, conductive adhesives or compression to a 2D electrode, or directly to the current collector [68].

Pletcher and Wills [29] initially experimented with carbon/high density polyethylene composites (C-



HDPE) onto which nickel foam and RVC were heat bonded. These could be modified by scraping away the attached layer after bonding, leaving behind a rough surface with Ni or RVC protrusions. The scraped RVC electrode was preferred as the positive electrode in early flow cell tests whilst the non-scraped Ni and RVC C-HDPE electrodes were preferred as the negative.

Various porosity grades and thicknesses of RVC positive electrodes, and both non-scraped 1 mm Ni and scraped Ni negative electrodes were reported by Wills *et al.* [17] in a flow cell employing 10 cm x 10 cm electrodes in a flow-by configuration (Section 10.1), with copper plates as current collectors. However, the experiments focus on other operating conditions and there is little discussion on the optimal electrode material, thickness and pore size. The authors here also reported the use of another carbon polymer: carbon/polyvinyl ester (Entegris GmbH). This composite material has also been reported elsewhere alongside a solid nickel plate as the negative electrode [16, 34]. These publications do not focus on the properties, merits and shortfalls of the electrodes.

Scraped Ni C-HDPE was used for the lead deposition studies discussed in Section 5.1. Plain C-HDPE was used for lead dioxide deposition discussed in Section 5.2. Scraped Ni C-HDPE was trialled as the positive electrode and it was found to be stable despite the highly oxidising potentials there. However, the adhesion of  $\text{PbO}_2$  was found to be poor, resulting in layers being dislodged from the electrode during flow cell cycling [32].

RVC is a versatile material available in various sizes and porosities. It has a low density and a honeycomb structure that offers a high surface area. It is structurally rigid in the presence of fluid flow, though its fragility can make it difficult to handle. It also possesses a low thermal expansion coefficient and good electrical conductivity. The corrosion resistance of RVC is good, but it is susceptible to degradation at high temperatures in oxidising environments [69]. Further properties

and uses of RVC have previously been reviewed by Arenas *et al.* [70].

Because of these qualities, RVC is a popular electrode material. In flow reactors, it can be an effective and economic alternative for the removal of metal ions from wastewater through electrodeposition, including  $\text{Pb}^{2+}$  [71]. It has also found use in fuel cells and batteries. Iacovangelo and Will [72] studied different grades of RVC in flowing zinc electrolytes. Using a flow-by configuration, deposition mainly occurred at the RVC surface and the interface between the RVC and graphite plate underneath. However, a high flow rate was found to improve the amount of zinc deposition throughout the RVC. By using a 2 mm thick RVC electrode, organic additives and a high flow rate ( $Re = 500$ ), dendrite-free zinc deposits were achieved deep into the pores, even at a high current density of  $100 \text{ mA cm}^{-2}$ .

Czerwiński and Żelazowska have studied the deposition of lead and lead dioxide onto RVC, concluding that each deposit behaved almost identically in terms of electrochemical behaviour to lead [73] and lead dioxide [74] respectively deposited onto a lead substrate, which was seen to be kinetically more favourable than onto a 2D glassy carbon rotating disc electrode (Section 4).

Recently, Oury *et al.* [67, 75] have reported the use of a novel 'pseudo-honeycomb' graphite positive electrode placed between two copper-plate negative electrodes. The electrolyte flows in through one of the negative electrodes, continuing through the holes in the positive electrode before finally exiting via the opposite negative electrode. The active surface area of the negative and positive electrodes is  $29 \text{ cm}^2$  and  $171 \text{ cm}^2$  respectively. Performance in general was good, achieving 95% and 75% charge and energy efficiencies respectively over 100 cycles, and the formation of passivating  $\text{PbO}_x$  layers (Section 5.5) was not detected. Despite the presence of 5 mM HDTMA in the electrolyte and a low operating current density, the negative copper electrodes were covered in a rough lead deposit composed of large, boulder-like nodules. Lead dendrites were also the primary cause of failure during cycling tests. This electrolyte composition is discussed further in Sections 8 and 9 and other SLFB

cell designs are discussed in Section 10.1.

RVC, carbon-polymer and nickel electrodes are the most widely reported in the SLFB literature. However, the effect of RVC on the phase composition of lead dioxide from MSA solutions remains to be explored. Cycling tests have so far been brief, limited by failure from shorting. Longer term studies are required to test the suitability of these electrodes but, at present, it is clear that 3D over 2D electrodes are favoured at both ends of the cell.

## 8 Electrolyte composition

### 8.1 Conventional electrolyte

Typically, a MSA-based lead plating bath contains  $200 \text{ g dm}^{-3}$  of lead ( $0.97 \text{ M Pb}^{2+}$ ) and  $100 \text{ g dm}^{-3}$  ( $1.0 \text{ M}$ ) of MSA. Deposition occurs at  $30 - 60 \text{ mA cm}^{-2}$  between  $293$  and  $303 \text{ K}$  with the use of organic additives [25].

It has been suggested by Oury *et al.* [67] that the  $\text{H}^+$  concentration never exceeds  $1 \text{ M}$  during cell operation due to the formation of insoluble, non-stoichiometric lead oxides which passivate the positive electrode surface, affecting cell longevity (Section 5.5). Using the novel pseudo-honeycomb cell design (Section 7), Oury *et al.* preferred an electrolyte consisting of  $1.0 \text{ M Pb}^{2+}$  and  $0.25 \text{ M MSA}$ , with  $5 \text{ mM HDTMA p-toluene sulfonate}$  and  $60 \text{ mM NaF}$ .

The most successful proof-of-concept study was conducted by Verde *et al.* [37]. The authors achieved 2000 cycles at 95% charge and 79% voltage efficiency using a  $0.7 \text{ M Pb}^{2+}$  and  $1.0 \text{ M MSA}$  electrolyte, albeit on a small scale unrepresentative of flow battery conditions.

The largest electrodes tested in a soluble lead flow cell is 1000 cm<sup>2</sup>. This was completed in a collaboration between C-Tech Innovation Ltd, E.On and the University of Southampton [76] (Section 10.1). Only limited results and information about the electrolyte composition is reported. This work follows on from experiments conducted by Wills *et al.* [17], where 100 cycles at close to 90% charge and 80% voltage efficiency were achieved (Section 9.1). The preferred electrolyte in both studies was 1.5 M Pb<sup>2+</sup> and 1.0 M MSA electrolyte, with 1 g dm<sup>-3</sup> of lignosulfonic acid.

## 8.2 Recycled electrolyte

Orapeleng *et al.* [77] have investigated methods to produce an electrolyte for the SLFB using Pb<sup>2+</sup> recovered from spent LABs, defined as having a state of health (SoH) of 80% or lower. Six electrolytes are compared. Each electrolyte is prepared by dissolving the LAB electrodes in 2.5 M MSA. Two electrolytes were prepared using each of the following conditions: 2.5 M MSA only, 2.5 M MSA and 0.09 M H<sub>2</sub>O<sub>2</sub>, 2.5 M MSA and 0.9 M H<sub>2</sub>O<sub>2</sub>. H<sub>2</sub>O<sub>2</sub> was used in order to oxidise the Pb electrode and reduce the PbO<sub>2</sub> electrode. One of the each pair of electrolytes was then heated to 303 K while the remaining electrolytes were heated to 313 K. Both electrolytes containing 2.5 M MSA and 0.9 M H<sub>2</sub>O<sub>2</sub> were shown to be able to successfully recover 0.9 – 1.5 M Pb<sup>2+</sup> over 6 hours. A ‘recovered’ electrolyte, consisting of 0.9 M Pb<sup>2+</sup> and 0.7 M MSA, was charged at 20 mA cm<sup>-2</sup> for 60 mins before being discharged at the same current density. The cell was cycled twenty times in total. The test was repeated using an equivalent electrolyte made from lead(II) methanesulfonate and methanesulfonic acid. Both electrolytes averaged 64% voltage efficiency, with the fresh electrolyte achieving 85% average charge efficiency compared to 81% with the recovered.

# 9 Performance

## 9.1 Flow cells

The soluble lead system has been scaled up to the 29 cm<sup>2</sup> and 100 cm<sup>2</sup> electrode scales. These have been subjected to constant current charge/discharge cycling each with unique electrodes and electrolytes. Table 2 summarises the results of these experiments.

Collins *et al.* [16] used a low Pb<sup>2+</sup> concentration of 0.5 M to simulate mass transport problems that could occur during cycling at higher states of charge. Aside from the study reported in Table 2, Wills *et al.* [17] conducted several other charge/discharge cycling tests with their 100 cm<sup>2</sup> cell, varying the current density between 10 and 100 mA cm<sup>-2</sup>, and involving electrodes of RVC, nickel foam (only at the -ve electrode) and carbon felt. Leit-C conductive carbon cement was used to attach the electrodes to the current collectors. Following charge, deposition is mentioned to be evenly distributed over and throughout the RVC electrodes, and in most cases there were no substantial growths along the internal cells walls at the edges of the electrodes (there is no discussion on whether the nickel foam was also coated evenly within). Different flow dispersion manifolds and turbulence promoters were also investigated to prevent the creep of PbO<sub>2</sub> and dendritic Pb growth (Section 10.1).

## TABLE 2 NEAR HERE

Performance is good in general, averaging  $\geq 65\%$  energy efficiency, but cycle life is limited by shorting caused by the contact between deposits. Collins *et al.* [16] were able to achieve only 40 cycles at 20 mA cm<sup>-2</sup>. They also achieved 19 cycles at 30 mA cm<sup>-2</sup> and 164 cycles at 10 mA cm<sup>-2</sup> in separate tests. The low current density and charge time used by Wills *et al.* ensured that Pb dendritic growth and PbO<sub>2</sub> creep was kept under control. Oury *et al.* recorded a 75% average energy efficiency across 100 cycles, despite the fact that shorting noise is reported as early as cycle 30. This shows that contact between deposits does not necessarily mean complete failure of the cell. The results presented

here represent the latest stage of SLFB development, and future work must aim to increase lifetime, efficiency, operating current density and charge/discharge duration.

## 9.2 Flow battery

The ICI FM01-LC is an electrochemical filter-press cell with an active electrode area of  $64 \text{ cm}^2$  ( $16 \text{ cm} \times 4 \text{ cm}$ ). It is designed for laboratory-scale experiments and the design is based on the industrial FM21-SP electrolyser used in the chlor-alkali industry [78]. It was adapted by Wills *et al.* [17] into a 2-cell bipolar SLFB stack and used for charge/discharge experiments. RVC and Ni foam was used for the positive and negative electrodes respectively and the electrolyte consisted of  $1.5 \text{ M Pb}^{2+}$  and  $1.0 \text{ M MSA}$ , with  $1 \text{ g dm}^{-3}$  lignosulfonic acid. After a series of conditioning cycles at  $20 \text{ mA cm}^{-2}$ , the stack was subjected to a series of 1 min charge/discharge cycles, where the current density was incremented by  $20 \text{ mA cm}^{-2}$  between 20 and  $160 \text{ mA cm}^{-2}$ . The stack potential at the end of each 1 min phase was recorded and plotted in potential vs. current density plots. This data was used to create power density vs. current density and stack potential plots on discharge, and this is presented in Figure 10.

The power density is seen to rise with current density, from  $50 \text{ mW cm}^{-2}$  at  $20 \text{ mA cm}^{-2}$  to a peak of  $308 \text{ mW cm}^{-2}$  at  $140 \text{ mA cm}^{-2}$ . In regards to the stack potential, the power density is relatively stable between  $1.6 \text{ V}$  and  $2.55 \text{ V}$  and the potential was seen to be equally split between the two cells, before decreasing at higher potentials beyond  $2.55 \text{ V}$  [17]. The system could therefore be able to charge and discharge at high current densities over short durations. It is best to avoid long charges at high current densities to avoid poor deposit formation. The soluble lead system could be discharged at higher rates over longer periods, but the effect of this on the deposit quality has not been explored.

## FIGURE 10 NEAR HERE

### 10 Flow cell engineering

#### 10.1 Cell design

Reviews of general flow cell engineering aspects has been published [8, 9] and this section introduces several important trade-offs for a soluble lead flow cell. The design of the flow cell must consider the need for a uniform current density and potential distribution across the electrode surface, sufficiently high and uniform mass transport rates, simplicity of design and ease of maintenance in relation to manufacturing and operating costs.

Electrodes should be held parallel to each other within the cell in order to establish a uniform electric field between them [53]. In the SLFB particularly, the interelectrode gap is an important trade-off; the space needs to be wide enough for deposits to form without electrically shorting the cell and to minimise the pressure loss, whilst also being small enough to minimise the potential drop across the electrolyte. The favoured width in the soluble lead flow cell is 1.0 - 1.2 cm; Collins *et al.* [16] were able to extend cell lifetime by increasing the width to 2.4 cm, as shorting was delayed, but at a cost of an increased potential drop and lower voltage efficiency.

From the Hagen-Poiseuille equation, it can be seen that pressure drop is greater when using highly viscous electrolytes. Therefore, because viscosity would decrease with SoC [50], the pressure drop could be expected to also decrease with SoC. However, there is also the effect of deposition at the electrodes to consider; at higher SoC, deposition narrows the interelectrode gap, which would have the effect of increasing the pressure drop.

Cells can employ a 'flow-by' and 'flow-through' electrode configuration. In a flow-by system, the electrolyte flows past the surface of an electrode (either 2D or 3D), through the inter-electrode or separator-electrode gap. In a 'flow-through' system, a 3D porous electrode is compressed between the separator and electrode, causing the electrolyte to flow through the porous electrode. The direction of the fluid motion can be parallel or perpendicular to the flow of current [53]. The latter is more commonly used in industrial reactors (and also the VRFB [79]). So far, SLFB research has preferred a flow-by configuration but the cell design of Oury *et al.* [67] can be classed as a flow-through, parallel to current direction, flow reactor (Section 7).

Shunt currents occur when the charge flows through the flow channels from cell to cell rather than through the bipolar electrodes. This leads to a non-uniform potential distribution amongst the stacks in the cells, and in hybrid flow batteries there would be a varying amount of deposition between inner and outer cells. Shunt currents can be minimised by increasing the resistivity of the flow path: by using a less conductive electrolyte or a narrower, longer flow path. However, the former would also reduce the voltage efficiency whilst the latter would increase the pressure drop [56].

Figure 11 presents three designs developed by Wills *et al.* and C-Tech Innovation Ltd [17]. The 10 cm x 10 cm electrodes would be attached in the centre of the frames, denoted by the labels (A), (B) and (C).

## **FIGURE 11 NEAR HERE**

The authors describe three cell configurations: (A) a silicone gasket providing a 'V'-shaped inlet and outlet path (used without the spiral inlets/outlets); (B) cell spacer frames incorporating a spiral



inlet/outlet manifold, plenum chamber and ringed distributor; (C) plastic mesh in the plenum chamber to promote flow turbulence. The spiral manifolds extend the flow path between cells in the stack, increasing pressure drop whilst reducing the shunt loss. However, the authors do not report studies on this and the cell was not tested in a multi-cell configuration. The non-conductive ringed distributor was seen to act as a scaffold for well-adhered  $\text{PbO}_2$  growth, leading to shorting. The authors avoided its use in later experiments and describe attaching an insulating polyester tape around the perimeter of both electrodes in order to prevent the growth and creep of deposits along the edges, but there is no more discussion regarding this. Particles of  $\text{PbO}_2$  dislodged from the electrode surface were also seen to accumulate at the bottom of the plenum chamber and over time were seen to form a gel-like sludge (Section 5.6). Apart from these observations, there is no other discussion on the preferred cell design.

A larger,  $1000 \text{ cm}^2$  cell was produced under a collaboration among C-Tech Innovation Ltd., E.On and the University of Southampton, with funding from the Department of Trade and Industry (DTI) [76]. This work highlighted several challenges alongside proposed solutions regarding the cell design. The flow through the inlets and outlets should be even, which could be achieved by using a calming section (plenum chamber) prior to the electrode surface. The dendritic growth at the inlet and outlets highlighted by Wills *et al.* [17] reduced by increasing the length of the lead electrode by 20 mm. An increased pressure drop leads to lower leakage currents and hence more uniform deposits. A low linear flow velocity is also proposed to improve the quality of the deposits at both electrodes.

An electrode size scale-up factor of 10 from previous work [17] was chosen in order to allow a near commercial-scale cell to be produced whilst remaining within the scale of readily available carbon composite electrodes. Details of cycling tests at this scale are vague: it is understood that four cells were stacked together and cycled at  $50 \text{ mA cm}^{-2}$ . The charging/discharging time is defined by the

authors as 'longer than 60 mins'. In these tests, shorting was observed after just 10 cycles, and this was attributed to a decreased effectiveness of HDTMA at this larger scale. The addition of sodium lignosulfonate alongside the HDTMA was seen to improve the cycle life to 40 cycles. Other than the effect on cycle life, there is only a limited amount of information presented on the construction and performance of the flow cell stack.

The DTI report also provides a financial analysis of a commercial SLFB. Economic assessment of the system predicts that if the cycle life can be improved whilst maintaining  $50 \text{ mA cm}^{-2}$  and an energy efficiency of 69% before losses from the power electronics, the system would cost £2275 per kW plus a further £80 per kW h. With economies of scale, this estimate decreases to £1075 per kW and £50 per kW h for MW scale units. This is now approaching the benchmark of Open Cycle Gas Turbines (OCGT) of £800 per kW assuming similar lifetimes. However, it is unclear how these costs were calculated.

## **10.2 Cell maintenance**

Most types of flow battery use different active species in the positive and negative half-cells, which are kept apart by a separator. However, crossover of ions and water molecules through the separator is inevitable, irrespective of the selectivity quality of the separator. This causes a loss in energy capacity and also affects the battery efficiency. Rebalancing is required to reverse these effects, and the difficulty of doing so depends on the active species [9].

This is not a problem in the SLFB, but a different type of maintenance is necessary. Selecting a suitable electrode material and optimising the cell design, operating conditions and electrolyte may minimise dendritic Pb growth or  $\text{PbO}_2$  creep, but in the case of any accumulation of deposits at the

electrodes as well as particles dislodging and falling into the electrolyte from, for example, external physical shocks or a fast flow rate, a strategy would be required to return the electrode and the electrolyte to the initial conditions.

The battery could be discharged at low current densities until the potential drops to 0 V, which would signify that the electrodes are completely free of deposits. Alternatively, the polarities could be switched and a low charging current applied, with the potential maintained below 0 V. This would preferentially oxidise Pb into  $\text{Pb}^{2+}$  at the new positive electrode rather than oxidising  $\text{Pb}^{2+}$  into  $\text{PbO}_2$  (and similarly for the new negative electrode) [27]. Alternatively, a faster method would be to short the electrodes across a low impedance shunt whilst circulating the electrolyte. Such strategies are employed in the zinc-bromine flow battery [80], where stripping cycles are employed to fully remove the zinc deposits from the negative electrode.

However, these techniques would not dissolve any dislodged particles suspended in the flow network. Hydrogen peroxide,  $\text{H}_2\text{O}_2$ , is known for its oxidative and reductive properties. Aliquots of 0.86 M  $\text{H}_2\text{O}_2$  were periodically added during a cycling test conducted by Collins *et al.* [34] following a discharge phase, with the cell on open-circuit. The lead dioxide in the electrolyte and on the electrode reacted instantly and soon dissolved completely. Lead deposits at the negative electrode were also seen to react but at a much slower rate. Nevertheless, the procedure successfully extended the cell lifetime and was capable of returning the system close to its initial condition. However, the average charge efficiency was seen to decrease over the cycles following the additions and was attributed to an excess amount of  $\text{H}_2\text{O}_2$  remaining in the electrolyte. Furthermore, though satisfied with the results, when considering the cost of  $\text{H}_2\text{O}_2$ , the authors did not find this to be an economical strategy. A more practical solution will be an area of future research.

## 11 Modelling and simulation

Over the last decade, computational modelling of flow batteries has accelerated due to the availability of multi-physics software and improved experimental data to validate the resultant simulations. In the case of redox flow batteries, many detailed models have been provided for the all-vanadium RFB [81, 82]. The modelling of hybrid RFBs has taken longer since they inherently need to consider solid phase formation and dissolution, or gas evolution at an electrode surface.

A model for the soluble lead redox flow battery has evolved from work in the authors' laboratory [35]. A model based on the conservation of mass, momentum and charge has been developed. This is a two-dimensional, transient model that considers transport and kinetic properties of charged species in water and the key side reactions of the soluble lead system respectively. This model is capable of accurately simulating cell potential vs. time during constant current charge/discharge cycling as well as rationalising the state of charge and describing concentration and local electrolyte velocity distributions over several full charge/discharge cycles. Complex behaviour due to the formation of an oxide layer on the positive electrode surface is also included in the model. The full charge/discharge behaviour over two cycles is simulated for several cases to rationalise the effects of applied current density on the charge/discharge behaviour and the efficiency of the cell.

A similar two-dimensional flow simulation has been created by Bates *et al.* [83], who have further developed the model to include the effects of temperature, initial  $[\text{Pb}^{2+}]$  and  $[\text{H}^+]$ , and applied current density on the electrode surface. To simplify the simulation, a constant concentration of the electrolyte is assumed. Experimental work partially validated the simulation and showed a close resemblance to the model results.

Nandanwar and Kumar have created two models of the SLFB. The first [84] is a two-dimensional model that uses the same standard governing equations for an electrochemical system. The model is able to simulate charge/discharge behaviour, including non-uniform current distribution on the electrode surface, and the effect of flow rate and flow direction. These simulations were performed on conventional planar electrodes as well as a system using annular cylindrical electrodes. The model also takes into account ion transport and resistance to ion transfer as well as non-uniform deposition on the electrodes. The simulation results lead to conclusions that a system with annular cylindrical electrodes and alternating the flow direction during charge and discharge would lead to a higher energy efficiency and a decreased rate of deposit build up when cycling.

The second work by Nandanwar and Kumar [85] uses the same set up with planar electrodes and looks specifically at what it refers to as the *coup de fouet* effect. This effect is the brief peak/trough in voltage at the beginning of each charge/discharge cycle. Other models assume highly conductive deposit layers. However, this work highlights that volume fractions below a certain critical limit for a conducting material in an insulating matrix, such as  $\text{PbO}_2$  in  $\text{PbO}$ , leads to the composite material to cease being conductive. As such, the composition and hence the conductivity of the deposit at the positive electrode must be taken into account. It is this change in conductivity of the positive deposit that is used to explain the *coup de fouet* phenomenon.

A system produced by Oury *et al.* [75] that uses a honeycomb positive electrode is described in Section 7. A two-dimensional approximation of this system using a series of parallel plates to describe the positive honeycomb structure has been produced by the same authors. Electrolyte flow and concentration, as well as current distributions, are simulated at a macroscopic scale across the entire two-dimensional model. The assumption of a compact, purely  $\text{PbO}_2$  positive layer leads to a simplification of the voltage profile when compared to experimental results. The voltages are

reasonable accurate and do show an increase in charge voltage for each subsequent cycle. However, the simulation results are only applicable to the first cycle and the final plateau of each subsequent charge cycle and the initial discharge voltages, due to the assumptions about the deposit at the positive electrode.

A major challenge for solid phase changes at electrode surfaces is the attendant shape change which can modify local flow, mass transport and active electrode area hence the time-dependent performance. In each of the studies mentioned in this section, the thickness of the deposit is assumed to be small compared to the cell dimensions and so is ignored. However, in high energy systems, this may not be true. These phase changes are partly dependent on electrolyte composition and nucleation/growth of phases on the electrode surface, which complicates electrolyte chemistry, electrolyte physical properties and deposit activity in an interactive fashion.

## **12 Conclusions and future work**

The soluble lead flow battery offers some advantages over other chemistries due to the single active species,  $\text{Pb}^{2+}$ . Lead is relatively low cost, readily available and recyclable within existing commercial supply chains, while methanesulfonic acid is less aggressive to component materials than sulfuric acid or strong alkaline electrolytes (for example KOH) typically found in other flow batteries. Energy efficiencies exceeding 75% and energy densities higher than those of the VRFB have been reported, though only when cycling at low depths of charge. The undivided SLFB requires just a single electrolyte, so the equipment needed to store and pump the electrolyte through the system is greatly reduced, potentially leading to significant cost reductions. Further cost savings occur due to the ability to operate without expensive separators.

The significant challenges with this system are related to the phase changes at both the positive and

negative electrodes. The morphology of the lead deposits must be controlled to avoid uneven or dendritic deposits, although the negative electrode reaction is efficient and has fast kinetics. Substantial issues occur at the positive electrode. Kinetics are much slower and the reversibility of the positive reaction is low. The formation of PbO within the deposit reduces the charge efficiency and affects the electrical conductivity of the positive electrode. Adhesion of PbO<sub>2</sub> to the electrode is also observed to be poor, leading to breaking away of the deposit from the electrode. It is likely that an ideal ratio of  $\alpha$ -PbO<sub>2</sub> and  $\beta$ -PbO<sub>2</sub> can improve the performance of the system by reaching a balance between a compact deposit (whilst remaining easy to discharge) and a porous deposit (without leading to breaking away of the deposit).

The conditions required to produce smooth and uniform lead and lead dioxide deposits have been discussed in relation to battery performance and is summarised in Table 3. As the parameter in the vertical column is increased from its lowest value,  $\uparrow$  represents that this has an effect of increasing or improving the corresponding horizontal property.  $\downarrow$  shows a negative effect. Pb deposit quality refers to a uniform, smooth deposit without the presence of dendritic growth or rocky clusters. PbO<sub>2</sub> deposit quality refers to a smooth surface without the presence of oxygen evolution damage, surface cracking or powdery deposits.

It is clear that several trade-offs are needed. Increasing [Pb<sup>2+</sup>] reduces ionic conductivity (if using high [MSA]), increases electrolyte viscosity and worsens the quality of the lead deposit. However, high [Pb<sup>2+</sup>] is required to minimise the competing oxygen evolution reaction at the positive electrode and to prevent a powdery PbO<sub>2</sub> deposit, whilst improving the energy capacity. Increasing [MSA] reduces the quality of both deposits and decreases the energy density by reducing the solubility limit of lead methanesulfonate. However, a high [MSA] is needed for a good solution conductivity which would reduce overall energy loss in the cell.

### TABLE 3 NEAR HERE

A high current density promotes dendritic Pb formation and leads to a poor PbO<sub>2</sub> quality, increasing the chances of surface cracking in highly acidic electrolytes. Whilst the temperature was seen to slightly increase the solubility limit and improve conductivity, the quality of the lead deposit fell. At the positive electrode, a high temperature saw the formation of  $\beta$ -PbO<sub>2</sub> dominant deposits, which were often powdery and weakly-adhering. Further work is required on relating the flow rate to cell performance in order to minimise the pumping power.

The majority of the work completed on the SLFB has been at single cell scale with an electrode area of less than 100 cm<sup>2</sup>. However, the battery has been scaled up to a four-cell 1000 cm<sup>2</sup> electrode-size, kW scale battery stack, though only limited results have been published. There is a significant amount of work still required for scale up of the SLFB, including developing specific charge/discharge regimes for long-term continual operation and overcoming sludge build-up, sloughing of active material from the electrode surfaces and reducing dendritic formations. Some modelling and simulation has been completed on the SLFB, however, more accurate simulations of the whole system are required in order to scale the system further. Specifically, models that incorporate the changing inter-electrode gap during charge discharge and species concentration gradients within the porous deposits and flow channel. This will identify the ‘safe’ current limits for charge and discharge as a function of state of charge. Electrode materials, cell and stack design remain to be optimised, including aspects to optimise the flow distribution and speed of electrolyte over the electrode while keeping pumping losses low taking into account the change in cell geometry due to the change in deposit thickness. A low-cost, effective maintenance cycle as an alternative to the addition of hydrogen peroxide should be developed, in conjunction with a battery management



system to allow for optimised operation over a long cycle lifetime.

Developments over the past five years have greatly enhanced the performance of the soluble lead system, with >1000 hours continuous charge/discharge operation reportedly achieved [37] and a more detailed understanding of the processes occurring in the lead dioxide deposits.. However, in order to move towards commercialisation of the technology, significant further work is still required. It is particularly important to adopt an electrochemical engineering approach to cell design and the effect of operational parameters on the reaction environment within the cell. Detailed local and spatial information on flow, current distribution and potential distribution across the surface of the electrodes is needed to optimise cell design and battery performance.

## **Acknowledgements**

The authors would like to thank the Department of Energy and Climate Change for their financial support as part of the PBatt project over the period this review was written.

## References

- [1] H. Chen, T. N. Cong, W. Yang, C. Tan, Y. Li, and Y. Ding, "Progress in electrical energy storage system: A critical review," *Progress in Natural Science*, vol. 19, pp. 291-312, 3/10/ 2009.
- [2] A. A. Akhil, G. Huff, A. B. Currier, B. C. Kaun, D. M. Rastler, S. B. Chen, *et al.*, "DOE/EPRI Electricity Storage Handbook in Collaboration with NRECA," Sandia National Laboratories (SNL-NM), Albuquerque, NM (United States) 2015.
- [3] M. Bartolozzi, "Development of redox flow batteries. A historical bibliography," *Journal of Power Sources*, vol. 27, pp. 219-234, 1989.
- [4] C. Ponce de León, A. Frías-Ferrer, J. González-García, D. A. Szánto, and F. C. Walsh, "Redox flow cells for energy conversion," *Journal of Power Sources*, vol. 160, pp. 716-732, 9/29/ 2006.
- [5] A. Weber, M. Mench, J. Meyers, P. Ross, J. Gostick, and Q. Liu, "Redox flow batteries: a review," *Journal of Applied Electrochemistry*, vol. 41, pp. 1137-1164, 2011/10/01 2011.
- [6] P. Leung, X. Li, C. P. De León, L. Berlouis, C. J. Low, and F. C. Walsh, "Progress in redox flow batteries, remaining challenges and their applications in energy storage," *Rsc Advances*, vol. 2, pp. 10125-10156, 2012.
- [7] W. Wang, Q. Luo, B. Li, X. Wei, L. Li, and Z. Yang, "Recent progress in redox flow battery research and development," *Advanced Functional Materials*, vol. 23, pp. 970-986, 2013.
- [8] L. Arenas, C. P. de León, and F. Walsh, "Engineering aspects of the design, construction and performance of modular redox flow batteries for energy storage," *Journal of Energy Storage*, vol. 11, pp. 119-153, 2017.
- [9] B. R. Chalamala, T. Soundappan, G. R. Fisher, M. R. Anstey, V. V. Viswanathan, and M. L. Perry, "Redox flow batteries: an engineering perspective," *Proceedings of the IEEE*, vol. 102, pp. 976-999, 2014.
- [10] *United States Department of Energy: Energy Storage Database (July 2016)*. Available: <https://www.energystorageexchange.org/>
- [11] A. Hazza, D. Pletcher, and R. Wills, "A novel flow battery: A lead acid battery based on an electrolyte with soluble lead(ii) Part I. Preliminary studies," *Physical Chemistry Chemical Physics*, vol. 6, pp. 1773-1778, 2004.
- [12] A. J. Bard, R. Parsons, and J. Jordan, *Standard potentials in aqueous solution* vol. 6: CRC press, 1985.
- [13] P. W. Atkins, *Physical chemistry*. Oxford: Oxford University Press, 1997.
- [14] L. P. J. Wallis and R. G. A. Wills, "Membrane divided soluble lead battery utilising a bismuth electrolyte additive," *Journal of Power Sources*, vol. 247, pp. 799-806, 2/1/ 2014.
- [15] A. Hazza, D. Pletcher, and R. Wills, "A novel flow battery: A lead acid battery based on an electrolyte with soluble lead(II) Part IV. The influence of additives," *Journal of Power Sources*, vol. 149, pp. 103-111, 9/26/ 2005.
- [16] J. Collins, G. Kear, X. Li, C. T. J. Low, D. Pletcher, R. Tangirala, *et al.*, "A novel flow battery: A lead acid battery based on an electrolyte with soluble lead(II) Part VIII. The cycling of a 10 cm×10cm flow cell," *Journal of Power Sources*, vol. 195, pp. 1731-1738, 3/15/ 2010.
- [17] R. G. A. Wills, J. Collins, D. Stratton-Campbell, C. T. J. Low, D. Pletcher, and F. C. Walsh, "Developments in the soluble lead-acid flow battery," *Journal of Applied Electrochemistry*, vol. 40, pp. 955-965, 2010/05/01 2010.
- [18] D. Pavlov, *Lead-acid batteries: science and technology*: Elsevier, 2011.
- [19] C. Vincent and B. Scrosati, *Modern batteries*: Elsevier, 1997.
- [20] *Battery University: How does the lead acid battery work? (October 2016)*. Available:

[http://www.battayuniversity.com/learn/article/lead\\_based\\_batteries](http://www.battayuniversity.com/learn/article/lead_based_batteries)

- [21] L. Lam and R. Louey, "Development of ultra-battery for hybrid-electric vehicle applications," *Journal of power sources*, vol. 158, pp. 1140-1148, 2006.
- [22] C. P. Zhang, S. M. Sharkh, X. Li, F. C. Walsh, C. N. Zhang, and J. C. Jiang, "The performance of a soluble lead-acid flow battery and its comparison to a static lead-acid battery," *Energy Conversion and Management*, vol. 52, pp. 3391-3398, 11// 2011.
- [23] J. H. Baldwin, E. J. Peebles, W. H. Power, and J. C. White, "Lead perchloric acid primary cell," ed: US Patent 2,492,206, 1949.
- [24] G. McDonald, E. Weissman, and T. Roemer, "Lead-Fluoroboric Acid Battery," *Journal of the Electrochemical Society*, vol. 119, pp. 660-663, 1972.
- [25] M. Schlesinger and M. Paunovic, *Modern electroplating* vol. 55: John Wiley & Sons, 2011.
- [26] F. Beck, "Lead batteries," ed: US Patent 4,001,037, 1977.
- [27] R. Wurmb, F. Beck, and K. Boehlke, "Secondary battery," ed: US Patent 4,092,463, 1978.
- [28] P. O. Henk and Z. A. Piontkowski, "Lead salt electric storage battery," ed: US Patent 4,331,744, 1982.
- [29] D. Pletcher and R. Wills, "A novel flow battery: A lead acid battery based on an electrolyte with soluble lead(ii) Part II. Flow cell studies," *Physical Chemistry Chemical Physics*, vol. 6, pp. 1779-1785, 2004.
- [30] D. Pletcher and R. Wills, "A novel flow battery: A lead acid battery based on an electrolyte with soluble lead(II) Part III. The influence of conditions on battery performance," *Journal of Power Sources*, vol. 149, pp. 96-102, 9/26/ 2005.
- [31] D. Pletcher, H. Zhou, G. Kear, C. T. J. Low, F. C. Walsh, and R. G. A. Wills, "A novel flow battery: A lead-acid battery based on an electrolyte with soluble lead(II) Part V. Studies of the lead negative electrode," *Journal of Power Sources*, vol. 180, pp. 621-629, 5/15/ 2008.
- [32] D. Pletcher, H. Zhou, G. Kear, C. T. J. Low, F. C. Walsh, and R. G. A. Wills, "A novel flow battery: A lead-acid battery based on an electrolyte with soluble lead(II) Part VI. Studies of the lead dioxide positive electrode," *Journal of Power Sources*, vol. 180, pp. 630-634, 5/15/ 2008.
- [33] X. Li, D. Pletcher, and F. C. Walsh, "A novel flow battery: A lead acid battery based on an electrolyte with soluble lead(II) Part VII. Further studies of the lead dioxide positive electrode," *Electrochimica Acta*, vol. 54, pp. 4688-4695, 8/1/ 2009.
- [34] J. Collins, X. Li, D. Pletcher, R. Tangirala, D. Stratton-Campbell, F. C. Walsh, *et al.*, "A novel flow battery: A lead acid battery based on an electrolyte with soluble lead(II) Part IX: Electrode and electrolyte conditioning with hydrogen peroxide," *Journal of Power Sources*, vol. 195, pp. 2975-2978, 5/1/ 2010.
- [35] A. A. Shah, X. Li, R. G. Wills, and F. C. Walsh, "A mathematical model for the soluble lead-acid flow battery," *Journal of The Electrochemical Society*, vol. 157, pp. A589-A599, 2010.
- [36] R. Clarke, B. Dougherty, S. Harrison, J. Millington, and S. Mohanta, "Battery with bifunctional electrolyte," ed: US Patent 6,986,966, 2005.
- [37] M. G. Verde, K. J. Carroll, Z. Wang, A. Sathrum, and Y. S. Meng, "Achieving high efficiency and cyclability in inexpensive soluble lead flow batteries," *Energy & Environmental Science*, vol. 6, pp. 1573-1581, 2013.
- [38] A. B. Velichenko, R. Amadelli, E. V. Gruzdeva, T. V. Luk'yanenko, and F. I. Danilov, "Electrodeposition of lead dioxide from methanesulfonate solutions," *Journal of Power Sources*, vol. 191, pp. 103-110, 6/1/ 2009.
- [39] D. Green and J. Maloney, "Perry's Chemical Engineers' Handbook," ed: McGraw-Hill Book Company, New York, New York, 1984.
- [40] J. Yan, *Handbook of Clean Energy Systems* vol. 5. New York: John Wiley & Sons Ltd, 2015.
- [41] X. Li, D. Pletcher, and F. C. Walsh, "Electrodeposited lead dioxide coatings," *Chemical Society Reviews*, vol. 40, pp. 3879-3894, 2011.

- [42] W. Mindt, "Electrical Properties of Electrodeposited PbO<sub>2</sub> Films," *Journal of The Electrochemical Society*, vol. 116, pp. 1076-1080, August 1, 1969 1969.
- [43] A. T. Kuhn, *The electrochemistry of lead*: Academic Press, 1979.
- [44] M. Pourbaix, "Atlas of electrochemical equilibria in aqueous solutions," 1974.
- [45] C. Rosenstein, "Methane Sulfonic Acid as an Electrolyte for Tin, Lead and Tin--Lead Plating for Electronics," *Met. Finish.*, vol. 88, pp. 17-21, 1990.
- [46] M. D. Gernon, M. Wu, T. Buszta, and P. Janney, "Environmental benefits of methanesulfonic acid . Comparative properties and advantages," *Green Chemistry*, vol. 1, pp. 127-140, 1999.
- [47] *Sigma Aldrich (May 2015)*. Available: <https://www.sigmaaldrich.com/united-kingdom.html>
- [48] F. C. Walsh and C. P. de León, "Versatile electrochemical coatings and surface layers from aqueous methanesulfonic acid," *Surface and Coatings Technology*, vol. 259, pp. 676-697, 2014.
- [49] D. P. Kelly and J. C. Murrell, "Microbial metabolism of methanesulfonic acid," *Archives of microbiology*, vol. 172, pp. 341-348, 1999.
- [50] M. Krishna, L. P. J. Wallis, R. G. A. Wills, D. Hall, and A. A. Shah, "Measurement of key electrolyte properties for improved performance of the soluble lead flow battery," *International Journal of Hydrogen Energy*, vol. 42, pp. 18491-18498, 2017/07/20/ 2017.
- [51] F. Wandschneider, S. Röhm, P. Fischer, K. Pinkwart, J. Tübke, and H. Nirschl, "A multi-stack simulation of shunt currents in vanadium redox flow batteries," *Journal of Power Sources*, vol. 261, pp. 64-74, 2014.
- [52] M. Fleischmann, J. Mansfield, H. Thirsk, H. Wilson, and L. Wynne-Jones, "The investigation of the kinetics of electrode reactions by the application of repetitive square pulses of potential," *Electrochimica Acta*, vol. 12, pp. 967-982, 1967.
- [53] F. C. Walsh, *A first course in electrochemical engineering*: Electrochemical consultancy, 1993, ISBN: 0 9517307 1 1.
- [54] I. Sirés, C. Low, C. Ponce-de-León, and F. Walsh, "The characterisation of PbO<sub>2</sub>-coated electrodes prepared from aqueous methanesulfonic acid under controlled deposition conditions," *Electrochimica Acta*, vol. 55, pp. 2163-2172, 2010.
- [55] C.-H. Yeh, C.-C. Wan, and J.-S. Chen, "Physical and electrochemical characterization of PbO<sub>2</sub> electrode prepared at different H<sub>2</sub>SO<sub>4</sub>/H<sub>2</sub>O/PbO ratios," *Journal of power sources*, vol. 101, pp. 219-225, 2001.
- [56] D. Linden and T. B. Reddy, "Handbook of Batteries. 3rd," ed: McGraw-Hill, 2002.
- [57] P. Rüetschi, "Influence of crystal structure and interparticle contact on the capacity of PbO<sub>2</sub> electrodes," *Journal of The Electrochemical Society*, vol. 139, pp. 1347-1351, 1992.
- [58] I. Petersson, E. Ahlberg, and B. Berghult, "Parameters influencing the ratio between electrochemically formed  $\alpha$ - and  $\beta$ -PbO<sub>2</sub>," *Journal of Power Sources*, vol. 76, pp. 98-105, 1998.
- [59] H. Y. Chen, L. Wu, C. Ren, Q. Z. Luo, Z. H. Xie, X. Jiang, *et al.*, "The effect and mechanism of bismuth doped lead oxide on the performance of lead-acid batteries," *Journal of Power Sources*, vol. 95, pp. 108-118, 3/15/ 2001.
- [60] M. Heinemann, H. Terpstra, C. Haas, and R. De Groot, "Electronic structure of  $\beta$ -PbO<sub>2</sub> and its relation with BaPbO<sub>3</sub>," *Physical Review B*, vol. 52, p. 11740, 1995.
- [61] H. Bode, *Lead-Acid Batteries*. New York: John Wiley & Sons Ltd, 1977.
- [62] R. Kiessling, "Lead acid battery formation techniques," *Digatron Firing Circuits*, p. 2, 1992. *Digatron, Industrie Elektronik GmbH, Tempelhofer Str. 12, D-5100 Aachen, Germany*. Available online at: [http://mathscinotes.com/wp-content/uploads/2012/12/lead\\_acid.pdf](http://mathscinotes.com/wp-content/uploads/2012/12/lead_acid.pdf) (Oct 17)
- [63] A. Oury, A. Kirchev, Y. Bultel, and E. Chainet, "PbO<sub>2</sub>/Pb<sup>2+</sup> cycling in methanesulfonic acid and mechanisms associated for soluble lead-acid flow battery applications," *Electrochimica Acta*, vol. 71, pp. 140-149, 6/1/ 2012.

- [64] J. Feng and D. C. Johnson, "Electrocatalysis of Anodic Oxygen-Transfer Reactions: Titanium Substrates for Pure and Doped Lead Dioxide Films," *Journal of The Electrochemical Society*, vol. 138, pp. 3328-3337, 1991.
- [65] J. Cao, H. Zhao, F. Cao, J. Zhang, and C. Cao, "Electrocatalytic degradation of 4-chlorophenol on F-doped PbO<sub>2</sub> anodes," *Electrochimica Acta*, vol. 54, pp. 2595-2602, 2009.
- [66] R. Amadelli, L. Armelao, A. Velichenko, N. Nikolenko, D. Girenko, S. Kovalyov, *et al.*, "Oxygen and ozone evolution at fluoride modified lead dioxide electrodes," *Electrochimica Acta*, vol. 45, pp. 713-720, 1999.
- [67] A. Oury, A. Kirchev, and Y. Bultel, "Cycling of soluble lead flow cells comprising a honeycomb-shaped positive electrode," *Journal of Power Sources*, vol. 264, pp. 22-29, 2014.
- [68] M. Chakrabarti, N. Brandon, S. Hajimolana, F. Tariq, V. Yufit, M. Hashim, *et al.*, "Application of carbon materials in redox flow batteries," *Journal of Power Sources*, vol. 253, pp. 150-166, 2014.
- [69] J. Friedrich, C. Ponce-de-León, G. Reade, and F. C. Walsh, "Reticulated vitreous carbon as an electrode material," *Journal of Electroanalytical Chemistry*, vol. 561, pp. 203-217, 2004.
- [70] F. Walsh, L. Arenas, C. P. de León, G. Reade, I. Whyte, and B. Mellor, "The continued development of reticulated vitreous carbon as a versatile electrode material: Structure, properties and applications," *Electrochimica Acta*, vol. 215, pp. 566-591, 2016.
- [71] J. Wang and H. Dewald, "Deposition of Metals at a Flow-Through Reticulated Vitreous Carbon Electrode Coupled with On-Line Monitoring of the Effluent," *Journal of The Electrochemical Society*, vol. 130, pp. 1814-1818, 1983.
- [72] C. D. Iacovangelo and F. G. Will, "Parametric study of zinc deposition on porous carbon in a flowing electrolyte cell," *Journal of The Electrochemical Society*, vol. 132, pp. 851-857, 1985.
- [73] A. Czerwiński and M. Żelazowska, "Electrochemical behavior of lead deposited on reticulated vitreous carbon," *Journal of Electroanalytical Chemistry*, vol. 410, pp. 55-60, 1996.
- [74] A. Czerwiński and M. Żelazowska, "Electrochemical behavior of lead dioxide deposited on reticulated vitreous carbon (RVC)," *Journal of Power Sources*, vol. 64, pp. 29-34, 1997.
- [75] A. Oury, A. Kirchev, and Y. Bultel, "A numerical model for a soluble lead-acid flow battery comprising a three-dimensional honeycomb-shaped positive electrode," *Journal of Power Sources*, vol. 246, pp. 703-718, 2014.
- [76] J. Collins, J. Bateman, and D. Pletcher, "Emerging Energy Technologies: Redox flow cells for intelligent grid management, TP No: TP/4/EET/6/I/22296," Department of Trade and Industry (DTI), 2009.
- [77] K. Orapeleng, R. G. Wills, and A. Cruden, "Developing electrolyte for a soluble lead redox flow battery by reprocessing spent lead acid battery electrodes," *Batteries*, vol. 3, p. 15, 2017.
- [78] F. F. Rivera, C. P. de León, J. L. Nava, and F. C. Walsh, "The filter-press FM01-LC laboratory flow reactor and its applications," *Electrochimica Acta*, vol. 163, pp. 338-354, 2015.
- [79] C. Yin, S. Guo, H. Fang, J. Liu, Y. Li, and H. Tang, "Numerical and experimental studies of stack shunt current for vanadium redox flow battery," *Applied Energy*, vol. 151, pp. 237-248, 2015.
- [80] D. M. Rose and S. R. Ferreira, "Initial test results from the RedFlow 5 kW, 10 kWh zinc-bromide module, phase 1," *Sandia National Laboratories Report 2012-1352, February 2012*, 2012.
- [81] A. Shah, M. Watt-Smith, and F. Walsh, "A dynamic performance model for redox-flow batteries involving soluble species," *Electrochimica Acta*, vol. 53, pp. 8087-8100, 2008.
- [82] A. A. Shah, R. Tangirala, R. Singh, R. G. A. Wills, and F. C. Walsh, "A Dynamic Unit Cell Model for the All-Vanadium Flow Battery," *Journal of The Electrochemical Society*, vol.

- 158, pp. A671-A677, June 1, 2011 2011.
- [83] A. Bates, S. Mukerjee, S. C. Lee, D.-H. Lee, and S. Park, "An analytical study of a lead-acid flow battery as an energy storage system," *Journal of Power Sources*, vol. 249, pp. 207-218, 2014.
- [84] M. N. Nandanwar and S. Kumar, "Modelling of effect of non-uniform current density on the performance of soluble lead redox flow batteries," *Journal of the Electrochemical Society*, vol. 161, pp. A1602-A1610, 2014.
- [85] M. Nandanwar and S. Kumar, "Charge coup de fouet phenomenon in soluble lead redox flow battery," *Chemical Engineering Science*, vol. 154, pp. 61-71, 2016.